



# The Bose-Einstein Condensate and Cold Atom Laboratory

Kai Frye<sup>1\*</sup> , Sven Abend<sup>1</sup>, Wolfgang Bartosch<sup>1</sup>, Ahmad Bawamia<sup>2</sup>, Dennis Becker<sup>1</sup>, Holger Blume<sup>3</sup>, Claus Braxmaier<sup>4,5</sup>, Sheng-Wey Chiow<sup>6</sup>, Maxim A. Efremov<sup>7,8</sup>, Wolfgang Ertmer<sup>1,9</sup>, Peter Fierlinger<sup>10</sup>, Tobias Franz<sup>11</sup>, Naceur Gaaloul<sup>1</sup>, Jens Grosse<sup>4,5</sup>, Christoph Grzeschik<sup>12</sup>, Ortwin Hellmig<sup>13</sup>, Victoria A. Henderson<sup>2,12</sup>, Waldemar Herr<sup>1,9</sup>, Ulf Israelsson<sup>6</sup>, James Kohel<sup>6</sup>, Markus Krutzik<sup>2,12</sup>, Christian Kürbis<sup>2</sup>, Claus Lämmerzahl<sup>4,14</sup>, Meike List<sup>9,14</sup>, Daniel Lüdtke<sup>11</sup>, Nathan Lundblad<sup>15</sup>, J. Pierre Marburger<sup>16</sup>, Matthias Meister<sup>7</sup>, Moritz Mihm<sup>16</sup>, Holger Müller<sup>17</sup>, Hauke Müntinga<sup>4,14</sup>, Ayush M. Nepal<sup>11</sup>, Tim Oberschulte<sup>3</sup>, Alexandros Papakonstantinou<sup>1</sup>, Jaka Perovšek<sup>4,5</sup>, Achim Peters<sup>2,12</sup>, Arnau Prat<sup>11</sup>, Ernst M. Rasel<sup>1</sup>, Albert Roura<sup>8</sup>, Matteo Sbroscia<sup>6</sup>, Wolfgang P. Schleich<sup>7,8,18</sup>, Christian Schubert<sup>1,9</sup>, Stephan T. Seidel<sup>1,19</sup>, Jan Sommer<sup>11</sup>, Christian Spindeldreier<sup>3</sup>, Dan Stamper-Kurn<sup>17</sup>, Benjamin K. Stuhl<sup>20</sup>, Marvin Warner<sup>4,5</sup>, Thijs Wendrich<sup>1</sup>, André Wenzlawski<sup>16</sup>, Andreas Wicht<sup>2</sup>, Patrick Windpassinger<sup>16</sup>, Nan Yu<sup>6</sup> and Lisa Wörner<sup>4,5</sup>

\*Correspondence:

[frye@iqo.uni-hannover.de](mailto:frye@iqo.uni-hannover.de)

<sup>1</sup>Institut für Quantenoptik, Leibniz Universität Hannover, Welfengarten 1, D-30167 Hannover, Germany  
Full list of author information is available at the end of the article

## Abstract

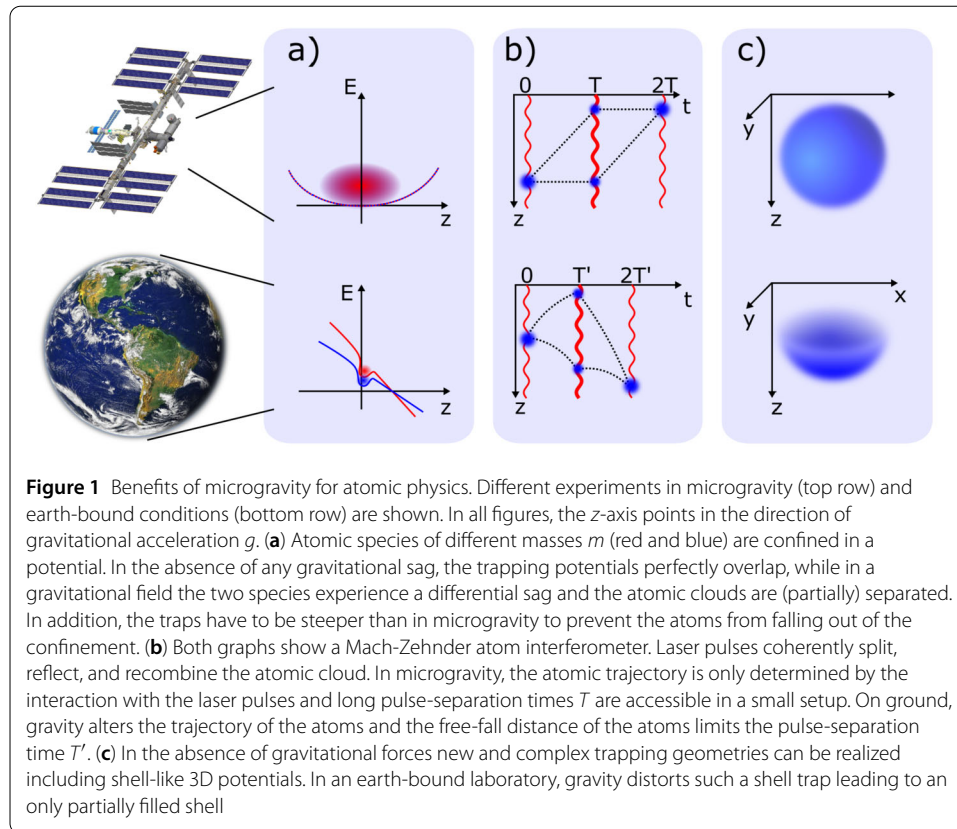
Microgravity eases several constraints limiting experiments with ultracold and condensed atoms on ground. It enables extended times of flight without suspension and eliminates the gravitational sag for trapped atoms. These advantages motivated numerous initiatives to adapt and operate experimental setups on microgravity platforms. We describe the design of the payload, motivations for design choices, and capabilities of the Bose-Einstein Condensate and Cold Atom Laboratory (BECCAL), a NASA-DLR collaboration. BECCAL builds on the heritage of previous devices operated in microgravity, features rubidium and potassium, multiple options for magnetic and optical trapping, different methods for coherent manipulation, and will offer new perspectives for experiments on quantum optics, atom optics, and atom interferometry in the unique microgravity environment on board the International Space Station.

**Keywords:** Bose-Einstein condensate; Quantum optics; Atom optics; Atom interferometry; Microgravity; International Space Station

## 1 Introduction

Laser cooling and the creation of Bose-Einstein condensates (BECs) [1] have opened up the field of dilute ultracold quantum gases. These systems enable the study of fundamental aspects of quantum mechanics, such as the evolution of matter waves [2], the transition of quantum statistic to classical thermodynamics [3], the impact of the dimensionality and topology of the gases [4] and may also probe the interface between quantum mechanics

© The Author(s) 2020. This article is licensed under a Creative Commons Attribution 4.0 International License, which permits use, sharing, adaptation, distribution and reproduction in any medium or format, as long as you give appropriate credit to the original author(s) and the source, provide a link to the Creative Commons licence, and indicate if changes were made. The images or other third party material in this article are included in the article's Creative Commons licence, unless indicated otherwise in a credit line to the material. If material is not included in the article's Creative Commons licence and your intended use is not permitted by statutory regulation or exceeds the permitted use, you will need to obtain permission directly from the copyright holder. To view a copy of this licence, visit <http://creativecommons.org/licenses/by/4.0/>.



and general relativity [5]. In a typical laboratory environment gravity deforms the trapping potentials and, in the absence of magnetic or optical fields, the atoms will simply fall towards the edge of the experimental chamber limiting the available free evolution times. Levitation techniques [6, 7] can compensate gravity, but can lead to unwanted systematic shifts in experiments, for example, additional phase shifts in atom interferometers, and they become technically more complex for multiple species with different atomic masses or internal states.

In microgravity, however, the atoms stay stationary with respect to the apparatus without the need for any external holding forces, thus enabling potentials without gravitational sag, long pulse separation times in atom interferometry [2] as well as the probing of surfaces with atoms over long times [8] and the realization of cloud geometries that are inaccessible in ground-based setups [4, 9] as illustrated in Fig. 1. Therefore, ultracold atoms in microgravity are ideal candidates to probe fundamental physics, such as testing the Einstein equivalence principle [5], investigating the validity of quantum mechanics on macroscopic scales [10], and probing dark energy [11–13] and dark matter [14–16]. Quantum sensors based on atom interferometry are considered for earth observation with satellite gravimetry [17], satellite gradiometry, and navigation in space [18]. Furthermore, a flexible, microgravity cold atom system is a critical pathfinder for the demonstration of other space borne atomic physics systems, such as highly-accurate optical frequency standards. While these applications inherently require space-borne operation, the conditions of microgravity also boost the potential performance of the proposed atom sensors.

The first microgravity experiment with ultracold atoms were realized in earth-based platforms such as the drop tower in Bremen [19, 20] and on parabolic flights [21, 22].

The precursor experiments to BECCAL began using the former platform, with the QUANTUS (Quantengase unter Schwerelosigkeit: quantum gases under microgravity) apparatus creating a BEC on an atom chip [19] and performing atom interferometry [20] during single drops, with a microgravity time of 4.7 seconds. The second generation of the QUANTUS apparatus was optimized to include a high-flux ultracold atom source [23] and to be operational in catapult mode, which almost doubles the time in microgravity. Another drop tower experiment realized all-optical evaporation in a dipole trap during free fall [24]. Most ground-based facilities are limited by repetition rate, for example, the drop-tower in Bremen only allows for 2-3 drops per day. To address this limitation, a novel facility, the Einstein Elevator in Hanover [25], is currently in the commissioning phase and will offer up to 100 shots per day, each with a free-fall time of approximately 4 s. It was designed to accommodate various payloads, including experiments on atom optics and interferometry, which may e.g. be utilised in searches for dark matter [26]. A BEC has already been demonstrated in a smaller Einstein Elevator [27].

To further increase the free-fall time one must move to space-based platforms, such as sounding rockets or satellites. In 2017, the MAIUS-I sounding rocket mission performed 81 experiments during six minutes of microgravity, including the first BEC in space [28] and experiments towards atom interferometry. Additional sounding rocket missions have acted as pathfinder demonstrations for the BECCAL and MAIUS laser systems. For example JOKARUS [29, 30], an Iodine frequency standard, contained the same generation of laser modules planned for use in BECCAL, and KALEXUS [31] which autonomously frequency-stabilised two lasers of a previous generation to the  $|F = 1/2\rangle \rightarrow F'$  crossover line of the  $D_2$  transition of  $^{39}\text{K}$ , demonstrating the laser performance and system development necessary for cold-atom experiments.

The International Space Station (ISS), on the other hand, provides a permanent microgravity environment. In May 2018, NASA launched the Cold Atom Laboratory (CAL) to the ISS [32, 33] and created the first BEC on an Earth-orbiting platform. This apparatus is designed to produce ultracold degenerate quantum gases of rubidium and potassium and to perform a vast range of experiments proposed by various researchers. Current topics include studies on few-body dynamics, magnetic lensing techniques [34], shell-geometry traps [4], alternative rf-outcoupling mechanisms [35], and quantum coherence for longer than 5 s. An upgrade to this apparatus was launched in December 2019 to add atom interferometry capabilities.

The Bose-Einstein Condensate and Cold Atom Laboratory (BECCAL), as presented in this paper, is a collaboration between NASA and DLR that will serve as a multi-user and -purpose apparatus to be installed on the ISS in the coming years. It is designed and will be built upon the experience and knowledge of QUANTUS, MAIUS, and CAL to offer higher atom numbers, an increased cycle rate, more complex optical and magnetic trapping strategies and improved atom-interferometry capabilities compared to predecessor experiments. The apparatus is designed to create BECs of  $^{87}\text{Rb}$  ( $^{41}\text{K}$ ) with more than  $1 \times 10^6$  ( $1 \times 10^5$ ) atoms. In addition, it will also provide the capability to create quantum degenerate gases of  $^{40}\text{K}$ . Thus, BECCAL will enable the study of scalar and spinor BECs as well as of mixtures of Bose-Bose and Bose-Fermi gases in absence of gravity. To detect these quantum gases after several seconds of free expansion, delta-kick collimation [34] will be employed to lower the expansion velocities of the atomic clouds. The apparatus will support the coherent splitting of matter waves separated by several centimeters and free

evolution times of several seconds. The atoms can be exposed to blue- and red-detuned optical fields for trapping, with arbitrarily-shaped potentials possible. This is a new feature for ultra-cold atom microgravity experiments, and will allow for versatile trapping and anti-trapping configurations.

Throughout its lifetime, BECCAL will perform a variety of experiments and serve as a pathfinder for future missions. This paper reports on the project, its envisioned scientific impact, and the design of the apparatus. The paper is organized as follows: Sect. 2 lays out the scientific envelope of the mission. The design of the instrument is detailed in Sect. 3, which includes an overview of the accommodation, budgets and safety measures (Sect. 3.1), the physics package (Sect. 3.2), the laser system (Sect. 3.3), the control electronics (Sect. 3.4), and the software architecture (Sect. 3.5). We present the installation, operation, and maintenance procedures in Sect. 4. The key features of the apparatus are summarized in Sect. 5, and the conclusion is given in Sect. 6.

## 2 Scientific envelope

Beyond principal mission targets such as the creation of BECs, the realization of low expansion velocities, and the demonstration of atom interferometry, a broader spectrum of experiments is anticipated. Therefore, BECCAL is designed to satisfy a wide range of experimental needs. The following sections outline several possible research topics and how they benefit from microgravity conditions. Operation in microgravity avoids the need for potentials for levitation and the associated inhomogeneities, especially for larger magnetic traps. Omitting magnetic fields for levitation additionally lifts the restriction of having the atoms in a specific state, enables experiments with mixtures of different states or species as well as tuning Feshbach resonances. Furthermore, microgravity avoids the non-uniformities of levitating heterogeneous gases in higher spatial dimensions (2D or 3D). The following parts focus on experiments which are either not realizable on ground or which are expected to show improved performance when transferred to microgravity. Some experiments presented here build upon and extend research that has been realized in QUANTUS [19, 20], MAIUS [28], CAL [32], and other microgravity activities [24, 27, 36].

### 2.1 Atom interferometry

Atom interferometry relies on the coherent splitting and recombination of matter waves to obtain an interference signal. This signal stems from the phase differences acquired on the interferometer paths. The phase differences depend on the potentials the atoms are subjected to, and on the chosen topology [37–40]. Atom interferometry is a versatile tool which can be used to probe fundamental physics [41–43], such as dark matter and dark energy theories [11–13, 44, 45], and to test the universality of free fall (UFF) [5, 36, 46–50]. Furthermore, it is possible to test the validity of quantum mechanics in extreme parameter ranges by creating coherent superpositions spanning over several tens of centimeters [10] or interferometer times larger than 10 s [51]. Atom interferometry also provides sensitive and accurate sensors for measuring rotations [52–55], Earth's gravitational acceleration [17, 56–62] for geodetic observations and offers new perspectives for navigation [18, 40, 63, 64].

Atom interferometers with optical or magnetic potentials as guides or for levitation against gravity have been extensively investigated, especially for compact sensors [51, 65–70]. These potentials, however, need to be well controlled, otherwise spurious phase shifts

will be induced which reduces contrast. Furthermore, even in an ideal setup, magnetic or optical levitation has limited uniform ranges, therefore, cannot support large area AI operation. Consequently, state-of-the-art atom interferometers used for precision measurements often avoid these challenges by using atoms in free fall [12, 48, 52, 59–61, 71], thus motivating this microgravity approach for BECCAL.

In a microgravity environment, the free fall of the atoms does not generally limit the total interferometer time. This allows for space and time separations of coherently split atoms which, on ground, are solely realizable in long baseline facilities [10, 48, 72]. Extended free-fall times can increase the sensitivity of atom interferometers. For the common Mach-Zehnder like [73] interferometer scheme, the phase scales with the squared pulse separation time. Microgravity also enables the operation of an atom interferometer that is stationary with respect to nearby objects in order to probe surface effects [74, 75] or to realize novel interferometry methods. A nadir pointing sensitive axis allows for measurement campaigns for mapping Earth's gravitational field [76–78] and UFF tests [79–81]. Furthermore, these activities serve as a pathfinder for future missions and applications, e.g. deep-space inertial sensing with atom interferometry, and as a gateway towards precision measurements of gravity, measurements of Newton's gravitational constant [71, 82], the gravitational Aharonov-Bohm effect [83] and gravitational wave detection [84–86].

## 2.2 Coherent atom optics

In order to reduce the expansion velocity of atomic clouds, BECCAL will exploit delta-kick collimation (DKC) techniques [34], in which a magnetic or optical potential is applied for a short period of time. This translates the kinetic energy of the atoms to potential energy and slows down the expansion velocity of the atomic cloud. The technique enables the preparation of atomic ensembles with expansion velocities smaller than  $100 \mu\text{m s}^{-1}$  [20, 87, 88], and consequently longer free evolution times. The lack of gravitational acceleration enables constant, highly controllable velocities of the atoms, which correspond to nearly monochromatic matter waves. These matter waves will be manipulated with various spatial- and temporal-dependent light fields to study basic phenomena of linear optics, but with switched roles – the matter acts as the wave and the light acts as the dispersive or absorptive medium. The latter depends on whether the scattering process is chosen to be coherent or incoherent and enables situations where light sheets diffract and refract matter waves.

For instance, a laser beam blue-detuned with respect to the atomic  $D_2$ -transition creates a repulsive potential and reflects the matter waves like a mirror. Two atom mirrors opposite each other form a matter-wave resonator. Microgravity conditions allow for full 3D symmetry of such a resonator so that atoms can be trapped in a 3D box potential, closely reproducing the textbook example of a particle in a box with infinitely high potential walls.

Another relevant topic is atom optics in the non-linear regime where homogeneous magnetic fields are applied to tune the scattering length of the atoms with the help of Feshbach resonances [89, 90] and to control the dispersion [91, 92]. For example, a negative scattering length creates a situation analogous to self-focusing. In addition, coherent matter-wave mixing will be possible, which enables a large set of new interferometric configurations.

Quantum reflection on surfaces represents another subject of interest. Here, a microgravity environment can help to improve the existing results [93] of quantum-mechanical

reflection of matter-waves from solid surfaces by providing smaller incident velocities and reduced mean-field interaction effects thanks to the shallow trapping possible in microgravity.

### 2.3 Scalar Bose-Einstein condensates

Scalar BECs will be studied in various magnetic and optical potentials, where the absence of gravity allows the creation of extremely shallow traps with trapping frequencies well below 1 Hz whilst maintaining atomic trapping. Since the critical temperature of Bose-Einstein condensation in a harmonic potential is proportional to the geometrical mean of the trapping frequencies, shallower traps result in a lower critical temperature. The critical temperature is the upper temperature limit of a BEC and lowering this threshold means that one can assure colder condensates [7]. This approach also leads to a decrease of the entropy of the gas, unlike adiabatic decompression techniques and DKC. The creation of spin excitations inside a BEC [94] further reduces the entropy and the momentum distribution of the thermalized magnons gives an estimate of the entropy. Hence, the creation of a gas with a record-low entropy per particle of  $S/N \leq 1 \times 10^{-4} k_B$  appears to be within reach in microgravity. Low-entropy gases are an essential resource for probing subtle many-body quantum effects and enhance the fidelity of quantum reflection on surfaces.

Magnetically trapped atoms can be transferred to an untrapped state via a weak radio-frequency field. In microgravity the dynamics of the outcoupled atoms are governed only by the repulsive atom-atom interaction giving rise to a slow expanding shell of atoms. This so-called space atom laser features an almost spherically-symmetric shape even if the initial BEC was confined in an elongated trap [35].

Another closely related topic is 3D bubble shells of trapped BECs [4, 9]. Here, a strong radio-frequency field dresses the trapping potential and hollows out the BEC. In this way a 2D BEC can be created embedded in a closed 3D shell. This process is solely realizable in microgravity and enables studies on thermodynamics and collective modes at a dimensional cross-over, edgeless surface excitations, and topological constraints on vortex dynamics in a curved geometry.

### 2.4 Spinor Bose-Einstein condensates and quantum gas mixtures

Spinor Bose gases are optically-trapped BECs where the spin of the atoms can be changed without losing the confinement. This is in contrast to magnetically trapped condensates, where the spin needs to be polarized properly to form a weak-field seeking state. Since the first realization of an optical dipole trap [95, 96], spinor Bose gases have been the subject of extensive research due to their interplay of magnetism and super-fluidity [97, 98]. In microgravity, the differential gravitational sag vanishes for different elements, isotopes and states enabling studies of spinor BECs and mixtures in unprecedented regimes.

For instance, optical box potentials with edge lengths of up to 100  $\mu\text{m}$  and particle numbers within reach of BECCAL lead to particle densities in the order of  $1 \times 10^{12} \text{ cm}^{-3}$ . This allows the study of magnetic interactions in a quantum fluid, such as spin-dependent  $s$ -wave collisions and spin-mixing dynamics. Increasing the volume of the trap lowers the densities of the atomic gases and allows the exploration of the non-interacting regime where the atoms are expected to show long-lived spin coherence. Thus, such an experiment has potential applications as a magnetic and rotation sensor, in addition to being a probe of fundamental physics.

Moreover, homogeneous magnetic fields enable the tuning of inter- and intra-species scattering lengths. The magnetic field strength can be chosen to enable the creation of strongly interacting mixtures independent of the trap volume [99]. Several Feshbach resonances may be accessible with reasonable magnetic field strengths to create hetero-nuclear spinor gases.

Furthermore, the combination of intercomponent attraction and intracomponent repulsion allows the formation of self-bound quantum gases, so-called quantum droplets [100–102]. These systems have never been studied in microgravity, which would enable the observation of the long-term dynamics of such droplets in a potential-free environment.

## 2.5 Strongly interacting gases and molecules

Strong atom-atom interactions often enhance three-body processes and fuel rapid atom loss. Microgravity increases the realizable interaction times due to the accessibility of extremely low densities and temperatures. In particular, the time-of-flight before the application of a magnetic lens determines the size of the atomic cloud and therefore controls its density. Additionally, the interaction volume can be chosen to be potential-free (e.g. a box trap generated by blue-detuned light) to create a homogeneous interaction strength over a large volume. Moreover, clouds of different atomic species perfectly overlap resulting in higher rates and efficiencies of Feshbach-molecule formation [103].

Ultra-low temperatures offer the energy resolution required for observing new features of Efimov physics [104, 105]. In addition, tuning the scattering rate with magnetic fields allows one to access a new regime, where two-body collisions are negligible with respect to three-body collisions, but without a high loss rate due to three-body recombination.

## 2.6 Quantum information

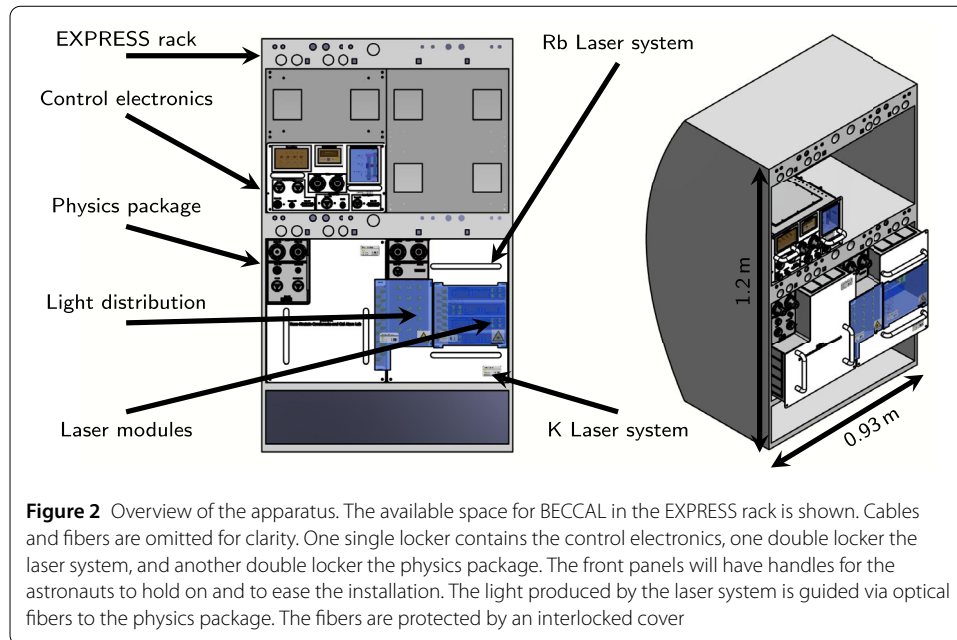
Dedicated experiments on quantum optics and atom optics may serve as a pathfinder and a major technology demonstrator for advancing quantum technology into space. This may enable future satellite-based quantum cryptography and quantum information/state transfer between distant points on Earth or beyond. In particular, cold-atomic ensembles could be useful for quantum information processing [106, 107] for space-based quantum communications applications [108, 109]. BECCAL's flexible cold atom platform will allow for demonstrations of techniques such as electromagnetically-induced transparency or coherent population trapping in ultracold ensembles for topics such as optical quantum memories and slow light [110].

## 3 Instrument design

In the following section the instrument design is presented, starting with an overview of the system, the restrictions set by the operation in orbit, and the requirements for safety. Subsequently the individual subsystems are explained in more detail.

### 3.1 Overview

BECCAL will be housed in the Destiny module on the ISS. The space station provides a standardized rack system to house payloads of different size and purpose, the so-called EXPRESS racks (EXpedite the PProcessing of Experiments to Space Station) [111]. Each EXPRESS rack offers eight standardized compartments and NASA allocates five of eight



lockers for BECCAL (Fig. 2). For implementation and due to launch restrictions, these five lockers will be separated into one single and two double lockers. The remaining locker spaces of the EXPRESS rack are occupied by other payloads. The accommodation in an EXPRESS rack therefore sets stringent requirements on volume, mass, external power, thermal management (Sect. 3.1.1), emitted radiation, and safety (Sect. 3.1.2).

The payload is divided into three subsystems – the physics package, the laser system, and the control electronics. The physics package, which contains the ultra-high vacuum system, where all the experiments on the atoms are carried out, is located in one double locker (Sect. 3.2). The other double locker contains the laser system and the laser electronics (Sect. 3.3). The single locker will house parts of the control electronics and the on-board computer (Sect. 3.4). The computer will run the experiment control software (Sect. 3.5) and will have additional hard drives for experimental data storage.

### 3.1.1 SWaP budgets

This section summarizes the available and chosen budgets for size, weight, and power (SWaP). Additionally, the thermal control system is outlined.

Compared to conventional quantum-optics-laboratory experiments, volume, mass, and power consumption of the apparatus are significantly reduced. The single locker has a size of 66 L and the two double lockers take 164 L each. The total mass is limited by the EXPRESS rack specifications to 328 kg [111].

The external power consumption depends on the operation mode and on the details of the experimental sequence. For more details on the power consumption see Sect. 3.4. An overview of the different operational modes is given in Sect. 4.

During operation, the payload generates thermal loads that will be dumped to the air cooling system of the EXPRESS rack and the ISS medium temperature water cooling loop. BECCAL's inner structure blocks the airflow through the system, which decreases the efficiency of the thermal transport, thus, most of the thermal load will be dissipated through the shared water cooling system. The maximum thermal load that can be dissipated is



therefore limited to comply with ISS interface requirements [111]. In BECCAL, each subsystem features two quick couplers and a piping system that enables water cooling of the installed heatsinks.

### 3.1.2 Safety

BECCAL is operated on board the ISS, and consequently in an environment designed for human space flight. While this offers unique opportunities for access, maintenance, manipulation, operation, and exchange of payloads, the safety and security of all parties involved, especially on orbit, is crucial. The safety requirements cover any risks for humans (i.e. by excess heat or radiation), especially for ISS crew members. Moreover, the safety of the space station has to be ensured and any interference (e.g. by electromagnetic radiation or vibrations) with other payloads needs to be minimized. Consequently, mitigating and preventing potential hazards and hazardous situations are design drivers for BECCAL. In particular, high voltage lines and free-space laser-light paths are contained within three levels of containment, such as interlocked containers and female sockets on the payload's front plates. All safety requirements and procedures are listed and referenced within reference [112].

BECCAL is operated from ground and does not require crew interaction in nominal operation. Even during installation and exchange operations, the lockers are not opened by the crew, who can only access the interfaces between the systems. The lockers are designed to prevent potential internal faults from propagating to the outside, this includes structural resilience, counter measures to block sharp objects entering the habitable volume, shielding against radiation (including light fields), and safeguards against excess surface temperatures.

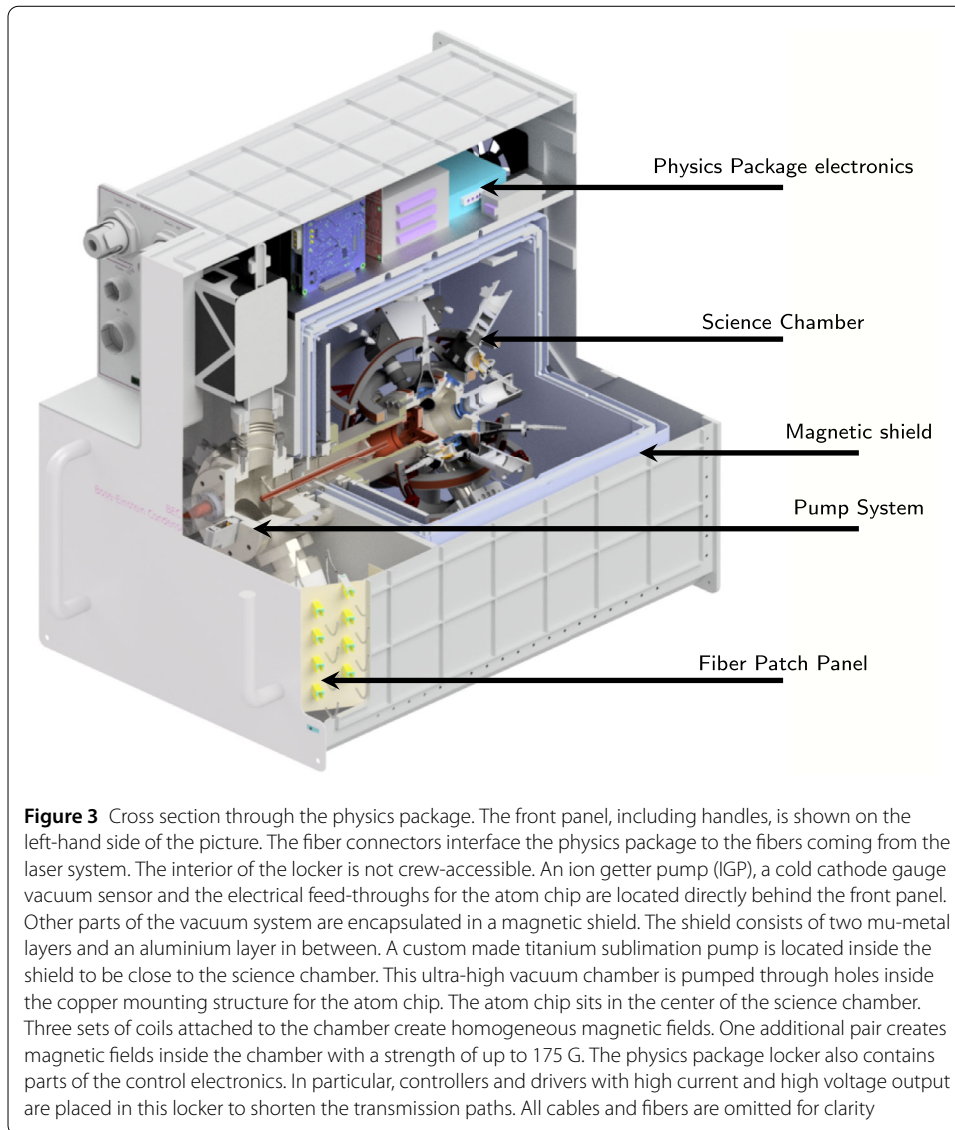
Electromagnetic interference of the experiment with the electrical devices on board the ISS potentially disturbs the experiment as well as the operation of the space station. The passive magnetic shielding (see also Sect. 3.2), which is commonly used to shield atomic physics experiments from external magnetic fields [113], also protects the ISS from the magnetic fields and radio-frequency radiation produced by the apparatus. The level of stray fields and radiation will be verified by a standard electromagnetic radiation test [112].

Like CAL, BECCAL will use rubidium and potassium as atomic sources. These elements are very reactive, radioactive with half lives of  $>1 \times 10^9$  years, and can be poisonous if swallowed or inhaled. However, the small amount of material used, and the enclosure inside several layers of protection, mitigates the radiation exposure of the crew and surroundings. Additionally, both alkali metals condense when exposed to ambient air pressures, reducing the probability of the release of large quantities of particles into the habitable area in the event of a breach in the vacuum system.

The requirements on radiation hardness against cosmic radiation are moderate compared to deep space missions due to the ISS's low orbit of 370 km to 460 km. Only single event effects need to be taken into account. Critical parts of the electronics will be radiation hard and shielded. All other circuits are designed to not go into over-current, short circuit or over-temperature, if a single component fails.

Temperature sensors are distributed all over the experiment, not only to detect over-temperature, but also to characterize any warm-up effects and the temperature distribution inside the payload [114].

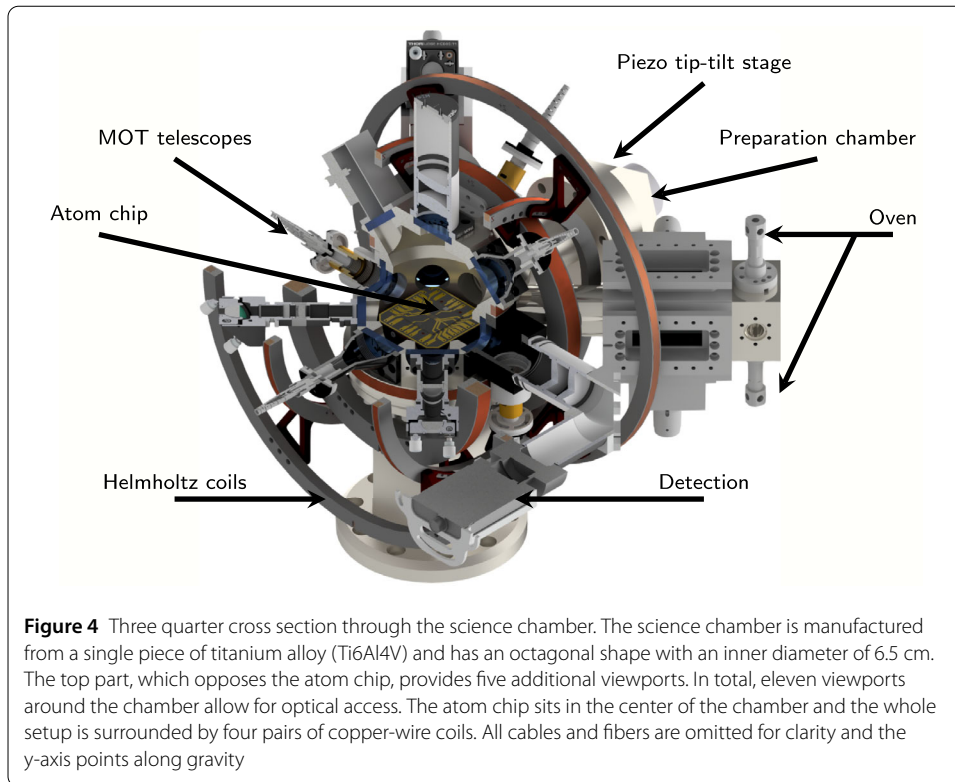
In addition to these passive mitigation strategies, the payload will be surveyed from ground during experimental operation. In standby the system will constantly check for key



parameters, such as vacuum quality, temperature levels, and drawn power, and alert the payload developer team and ISS personnel if a parameter exceeds the acceptable range for nominal operation. Moreover, the payload shuts down automatically before a hazardous situation arises due to overheating.

### 3.2 Physics package

The physics package is the subsystem where the experiments on the atoms are performed (Fig. 3). It contains the ultra-high vacuum system, which consists of several connected vacuum chambers, which are adapted from QUANTUS [23] and MAIUS setups [28]. In the preparation chamber, atomic gases of rubidium and potassium are cooled to form a cold atomic beam, which points into the science chamber (Sect. 3.2.1). This chamber supports trapping, cooling, and manipulation of atomic clouds (Sect. 3.2.2). The two-chamber design allows for evaporation, preparation, and transport of the atoms while simultaneously maintaining the ultra-high vacuum in the science chamber. The science chamber is surrounded by wire coils, which produce magnetic fields (Sect. 3.2.3) in com-



bination with the atom chip. Atom interferometry can be performed in two orthogonal axes (Sect. 3.2.4). Also attached to the science chamber are the setup for the creation of arbitrary shaped optical potentials (Sect. 3.2.5) and the detection system (Sect. 3.2.6). The vacuum pressure inside the chambers is maintained by several pumps, which are described in Sect. 3.2.7.

### 3.2.1 Science chamber

The science chamber has an octagonal shape (Fig. 4) and is manufactured from a titanium alloy (Ti6Al4V). The chamber features several ports for optical access and vacuum connectors—a total of six viewports and two vacuum connections as well as a top part with five additional viewports. It contains an atom chip and the tip-tilt mirror used for atom interferometry (Sect. 3.2.4).

Four viewports are available as optical access for magneto-optical trap (MOT) beams and for the absorption detection system (Sect. 3.2.6). Two beams are reflected by the surface of the atom chip. Two viewports perpendicular to each other will be used for the creation of painted, blue-detuned optical potentials (Sect. 3.2.5). The light for a red-detuned crossed optical dipole trap will be transmitted through two viewports. The two ports facing nadir are used for atom interferometry. One of those two ports provides an extension to the vacuum system to house the tip-tilt stage, and the other contains a window through which the atom interferometry beams enter the chamber. All the optical components are directly mounted onto the chamber to provide the required pointing stability. The fiber collimators contain additional photodiodes for power and polarization monitoring.

### 3.2.2 Atomic source

This section describes the creation of ultracold atomic clouds of rubidium and potassium. First, we comment on the choice of elements. Then we lay out the route for rapid production of quantum degenerate gases.

Rubidium and potassium were chosen for several reasons: (i) The strong  $D_2$  transition lines of rubidium and potassium are only 13 nm apart. An optical broadband coating with that range is easy to manufacture and is found in many commercial off-the-shelf optics. Thus, the same optics can be used for both elements which reduces the complexity of the apparatus substantially. (ii) The interspecies interaction can be tuned by using the rich spectrum of Feshbach resonances at moderate magnetic field strengths. (iii) There is roughly a factor of two in mass difference which makes the combination of those two elements interesting for potential tests of the universality of free fall. (iv) Potassium offers bosonic and fermionic isotopes, which facilitates the study of Bose-Bose and Bose-Fermi gases of different species. (v) Both species are currently being used in the MAIUS-B experiment [115], which features a similar atom chip, as well as in the CAL experiment. BECCAL will profit from this experience.

The cooling of the atoms takes place in two chambers. A  $2D^+$ -MOT configuration [116] creates a cold atomic beam in the preparation chamber. This beam will load a 3D-magneto-optical trap in the science chamber through a differential pumping stage. We expect the flux of  $^{85}\text{Rb}$  and  $^{87}\text{Rb}$  into the 3D-MOT to be  $1 \times 10^9$  atoms/s each, which was already shown in a similar setup [23]. The flux for  $^{39}\text{K}$  ( $^{41}\text{K}$ ) is expected to be roughly a factor of 10 (100) lower than for rubidium. The preparation chamber is directly connected to the ovens. One oven contains 1 g rubidium, the other 1 g potassium, both in natural abundance. An additional dispenser will contain 100 mg of enriched  $^{40}\text{K}$ . These samples are sufficient to last the whole mission duration.

Together with the magnetic field, four light beams form the 3D-MOT. Two light beams are reflected by the coated surface of the atom chip with an incident angle of  $45^\circ$ . We expect the MOT to provide  $2 \times 10^9$   $^{87}\text{Rb}$  atoms,  $1 \times 10^9$   $^{85}\text{Rb}$  atoms,  $8 \times 10^8$   $^{39}\text{K}$  atoms,  $4 \times 10^8$   $^{41}\text{K}$  atoms and  $1 \times 10^7$   $^{40}\text{K}$  atoms for single species operation each. The subsequent cooling steps are discussed in detail in Ref. [23], while here, a short outline is given. The 3D-MOT is followed by a phase of compressed MOT, with lower magnetic fields and higher detuning. This results in a higher density than in the initial MOT. The magnetic fields are then switched off and the cloud is cooled with polarization-gradient cooling. A shallow Ioffe-Pritchard magnetic trap with large trapping volume captures the atoms and subsequently the magnetic field gradients are increased. This tight trap allows for fast evaporation as a consequence of the increased collision rate in the dense cloud. The evaporation efficiency is such that there will be more than three orders of magnitude gain in phase-space density for every order of magnitude in atom loss. We expect to create single-species Bose-Einstein condensates of  $^{87}\text{Rb}$  and  $^{41}\text{K}$  with more than  $1 \times 10^6$  and  $1 \times 10^5$  atoms, respectively. For the creation of a dual-species BEC, the atoms are loaded into an optical dipole trap after a short period of evaporation. The Feshbach field is switched on to reduce two- and three-body losses and optical evaporation is performed. For mixtures the atom numbers are expected to be one order of magnitude less than for single species BECs. Magnetic trapping of the fermionic isotope of potassium will be realized for at least  $1 \times 10^4$  atoms with a Fermi fraction ( $k_b T/E_f$ ) of  $\leq 1$ .

For further manipulation, the atoms can be transferred into various magnetic traps (Sect. 3.2.3) and optical traps (Sect. 3.2.5). The atoms can be subjected to an magnetic [34] or optical delta-kick collimation to reduce the expansion velocity to values  $\leq 100 \mu\text{m s}^{-1}$ .

### 3.2.3 Atom chip and magnetic fields

The magnetic fields are created by an atom chip inside the science chamber and by copper wire coils outside the chamber in Helmholtz configuration. The atom chip is a versatile and compact tool for generating magnetic fields [6, 23]. Its design is adapted from the QUANTUS-2 apparatus [23]. It consists of one layer with mesoscopic copper wire structures and two layers of microscopic wire structures. The atom chip will feature  $1 \text{ mm}^2$  surfaces off-center with different electrical properties to study quantum reflection. Since the atoms are only a couple of hundreds of micrometers to a few millimeters away from the atom chip surface, high gradients can be realized with lower power than with a coil setup outside the vacuum chamber. High trap frequencies (up to 2 kHz) can be achieved with a few amperes of current, which makes evaporative cooling fast and power efficient. Most structures on the chip are made from single wires, which results in much lower inductance than in a coil setup. This makes switching times shorter than 100  $\mu\text{s}$  possible.

In order to create the quadrupole fields required to operate a MOT or Ioffe-Pritchard-type magnetic traps, the field created by the atom chip itself needs to be overlapped with homogeneous bias fields. In this setup, the homogeneous fields are created by three Helmholtz coils outside the vacuum chamber; one pair for every direction. The center of the harmonic traps can be chosen to be 0.1 mm to 2 mm away from the chip surface with aspect ratios of 100 : 100 : 1 to 2 : 2 : 1. An additional set of four coils produces homogeneous fields of up to 175 G for tuning the scattering length of the atoms. This field can be modulated with an on-top amplitude of 0 G to 1 G and frequencies up to 100 Hz, to enable fast hopping into or across Feshbach resonances.

Additional structures on the atom chip will be connected to a radio-frequency and a microwave source to facilitate forced evaporative cooling and state preparation. The atom chip and offset coils can be utilised for the generation of a three-dimensional magnetic trap and a radio-frequency field to create dressed potentials for shell-shaped traps as described in Refs. [4, 9, 117]. Combining this type of trap with an optical potential, using either of the optical dipole traps in BECCAL (see Sect. 3.2.5), enables the implementation of ring traps as discussed in Refs. [118, 119].

The science and the preparation chambers and the coils are located within a three-layer magnetic shield: two layers of mu-metal with a layer of aluminum in between. Mu-metal is a soft-ferromagnetic alloy commonly used for magnetic shielding due to its high permeability. The magnetic shielding factor will be roughly 300 for static fields and several orders of magnitude higher for oscillating fields.

### 3.2.4 Atom interferometry setup

BECCAL will have two independent atom interferometry axes. The primary axis is parallel both to Earth's acceleration (nadir) and the surface of the atom chip. The beam will be reflected by a mirror inside the vacuum apparatus. The second interferometry axis is perpendicular to the first and the beam is reflected by the atom chip. The  $1/e^2$  beam waist will be 6 mm for both axes.

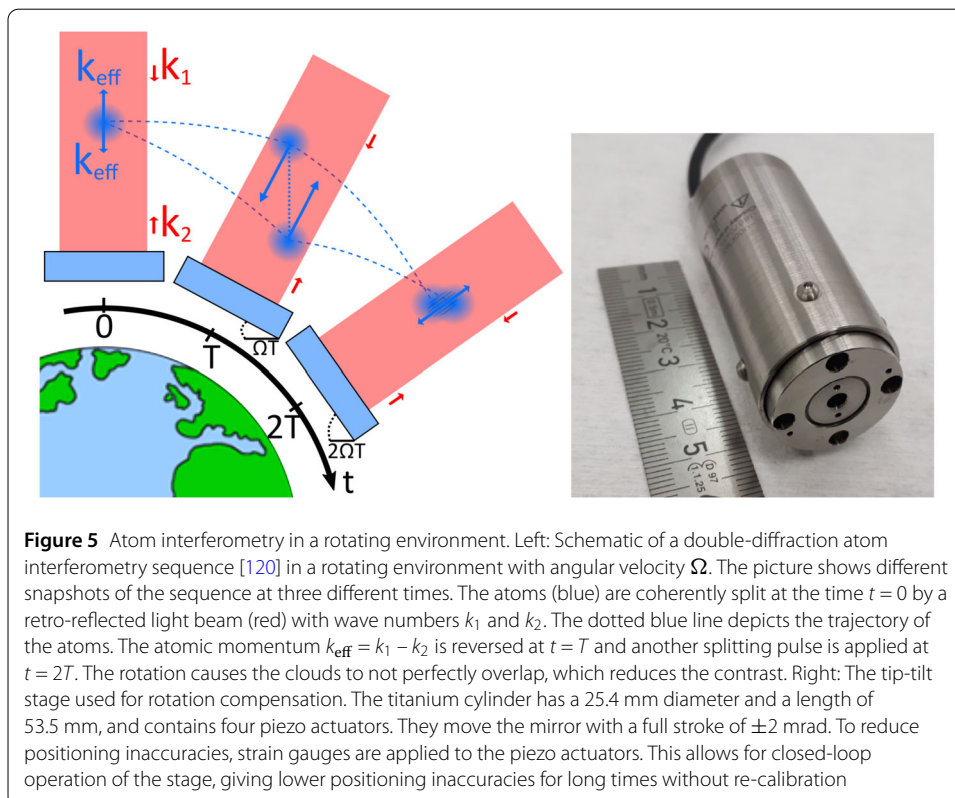
Auxiliary sensors will be used to characterize the environment and for correlation with the atom interferometers. These comprise an accelerometer and a gyro sensor which will

be placed in the vicinity of the vacuum system. The science chamber, and in particular the atom chip, will be equipped with a grid of temperature sensors. The temperature data will be used to model acceleration due to black body radiation [114].

The primary interferometer axis is parallel to the earth's gravitational acceleration, which enables the determination of the differential Eötvös ratio for rubidium and potassium [5]. The light beam enters the chamber via a window, interacts with the atoms, then passes through a quarter-waveplate, is retro-reflected by a mirror and passes through the same waveplate again before interacting with the atoms again. The waveplate rotates the parallel linear polarization of the two incident light fields by  $180^\circ$ , to enable double-Raman diffraction beam splitters [120].

Wavefront distortions are one of the limiting factors for the accuracy of atom interferometers [59, 61]. The distortions introduced to the light before interacting with the atoms are common to both the incident and counter-propagating beams. They are therefore suppressed in most atom interferometry configurations. However, this is not the case for distortions introduced by optics behind the atoms in the optical path. To minimize this, the retro-reflecting mirror and the waveplate will be designed to have a global flatness of  $\lambda/20$  and a local root mean squared surface roughness of  $\lambda/100$  and will be placed inside the vacuum chamber.

The ISS orbits the earth with an angular velocity of  $\Omega = 1.1 \text{ mrad s}^{-1}$ . Therefore, without any counter-rotating device for the interferometry mirror, the orbiting motion of the ISS will eliminate the contrast of the interferometry fringes completely (Fig. 5). While the systematic errors can in principle be accounted for in post-correction, the loss of contrast due to rotation is irretrievable. The contrast for a pulse separation time of 900 ms will be



below 0.2% [121] when assuming an atom interferometer using a  $^{87}\text{Rb}$  BEC with a mean velocity spread of  $100 \mu\text{m s}^{-1}$  and a Thomas-Fermi radius of  $150 \mu\text{m}$ . It has been shown that counter-rotating the interferometry mirror against external rotations is an effective method to regain contrast [122]. To this end, in our setup, the interferometry mirror sits on top of a moving stage driven by piezo actuators. This stage allows the mirror to rotate in two dimensions ('tip' and 'tilt'), which corrects wavefront tilt in two dimensions. Figure 5 (right) shows the custom design created in collaboration with *Physik Instrumente*. The rotating mirror will compensate the rotation of the ISS for the required 2.6 s total interferometry time.

The compensation of the rotation with a tip-tilt mirror implies a change in the effective wavenumber between the subsequent atom-light interactions of an interferometer pulse sequence. Fortunately, the combination of gravity gradients and these residual rotational effects can be effectively mitigated with the technique proposed in Ref. [123] and experimentally demonstrated in Ref. [124]. For total interferometer times of  $2T = 2.6 \text{ s}$  this involves changing the single-photon frequencies by  $\Delta\nu \approx 1.5 \text{ GHz}$  for the mirror pulse in a Mach-Zehnder interferometer [125].

### 3.2.5 Optical potentials

The apparatus will support experiments requiring light fields red- or blue-detuned to the  $D_2$  transition, with arbitrary shaping possible with the blue-detuned optical potentials. Blue-detuned potentials enable trapping the atoms in the dark region of a geometry, which results in a homogeneous trap [3] with low atom-light scattering rates [126].

Two options for the creation of highly controllable optical potentials are investigated for use in BECCAL. One option is the use of 2D acousto-optical deflectors (AODs), which deflect a beam of light in any transverse direction with an adjustable angle. By steering the beam much faster than the trap-frequency of the atomic trap, the atoms will see a time-averaged potential [127–129]. The refreshing rate of every possible shape shall be above 100 Hz in order to produce a time-averaged static potentials for the atoms. Another option is the use of spatial light modulators (SLMs). They imprint a phase onto a light beam to change the intensity distribution at a certain point in space [130, 131]. Both option enable the creation of blue-detuned optical traps with a tunable inner diameter from  $20 \mu\text{m}$  to  $1500 \mu\text{m}$ . The (time-averaged) barrier height will be  $5 \mu\text{K}$  for a contour length of  $\leq 100 \mu\text{m}$  and decrease for larger traps. In addition, the optical barrier can be moved with a speed of up to  $5 \text{ mm s}^{-1}$ .

The red-detuned light is used to create a crossed optical dipole trap [95, 96]. One beam of this trap can be steered with an AOD to ensure the overlap of the beams. The center of this trap is located 2 mm away from the atom chip surface. The focal point will have a waist of  $100 \mu\text{m}$  and the potential depth is tunable from  $0.01 \mu\text{K}$  to  $5 \mu\text{K}$ . Deep optical dipole traps are not required because the trap does not need to support the atoms against gravity. It will be possible to add a retro-reflection of one beam to create an optical lattice prior to every experimental run.

### 3.2.6 Detection

Virtually every experimental sequence in BECCAL will conclude by measuring an atomic signal. The apparatus will feature two acquisition methods. The first is a fluorescence detection system based on collecting photons that the atoms emit after an excitation. We

utilize a system of multiple lenses with a large numerical aperture for  $2f - 2f$  imaging with  $f$  being the focal length of the lens system. This creates an image of the atoms on a photo diode. The scheme uses near-resonant light and is state- and species-dependent. It will be used to obtain loading and lifetime curves of the atomic clouds as well as a state-selective readout for interferometry [5].

The second detection method relies on the atomic absorption of photons from an illuminating laser beam. A camera will take images of the laser beam with and without the shadow of the atomic cloud to gain information of the cloud's density. Two perpendicular absorption imaging systems will provide 3D information of the size and the shape of the atomic cloud. Each absorption detection system consists of a collimator to provide the illumination light. On the opposite side of the chamber is a lens systems which will focus the absorption images of the atoms onto a camera sensor. In addition to static lenses, we will utilize electrically tunable lenses to have a variable focal length  $f$ . In principle, the imaging system also resembles a  $2f - 2f$  scheme, but with two lenses. The first lens is optimized to minimize spherical aberrations and sits  $2f$  away from the atoms. The second lens sits close to the camera and is electrically tunable. For this purpose, we utilize a shape-changing lens from *optotune* with an optical fluid, which is sealed off with an elastic polymer membrane. This lens changes the focal length of the imaging systems by  $\pm 5$  mm and allows us to image the atoms in different positions with a resolution  $\leq 10$   $\mu\text{m}$ . Additionally, the depth of field will be adjustable from 100  $\mu\text{m}$  to 2000  $\mu\text{m}$ . This is especially useful for quantum reflection experiments as the different surfaces are off-center with respect to the atom chip. Furthermore, the investigation of hollow BECs will profit from this feature since the focus can be shifted to the surface of the shell.

### 3.2.7 Infrastructure

The science chamber will be continuously pumped by an ion getter pump (IGP) and a passive titanium sublimation pump. The combination of these pumps allows for the effective pumping of different species and maintains a vacuum quality in the order of  $1 \times 10^{-10}$  mbar throughout the operation of BECCAL. To maintain the vacuum during times of standby, the IGP is operational at all times. At regular intervals, and to increase the vacuum quality should it be needed, the titanium sublimation pump will be activated.

As the IGP produces strong magnetic fields, it is mounted outside the magnetic shield alongside an access port for the cables, and a vacuum sensor. The entirety of this system is called the pumping cube. The pumping cube is also the access point for the roughing pump, which is installed during integration to establish the required vacuum quality for the IGP. As the roughing pump is both large in volume and high in mass it is not transported to the ISS but pinched off before launch.

The launcher will not provide electrical power. Consequently, the active vacuum pump is switched off during this period of highest mechanical load, i.e. integration into the launcher, launch, and transport to the ISS. In combination with the absence of the roughing pump in orbit, a strong limit is set on this unpowered duration. In order to allow for the re-activation of the IGP in orbit, the vacuum system is designed to keep the pressure below  $1 \times 10^{-5}$  mbar, even under the conditions described above.

Control electronics for the atom chip, the coils, the high voltage power supply for the IGP, and auxiliary vibration, rotation and magnetic field sensors are also located outside of the magnetic shield. The controller for the IGP sits close to the pump so that the high voltage line is very short.



Electrical connectors are embedded in the outer locker case to provide connections for the control electronics subsystem and for the scientific data to be sent from this subsystem to the data storage device. There are also seventeen optical fiber connectors which will be used to connect the laser system and the physics package.

### 3.3 Laser system

All light fields required for BECCAL are generated and controlled within the ‘laser system’ subsystem. This system (including its associated control electronics) occupies one EXPRESS rack double locker. The generated light is delivered to the physics package via polarization-maintaining single-mode optical fibers. Within this section, we will outline the capabilities of the laser system, the architecture, and describe the main technologies used within the laser system, including the lasers, the free-space optics and the fiber optics.

#### 3.3.1 Laser system capabilities

The laser system must deliver light to seventeen separate optical fibers to the physics package in order to facilitate the ambitious functionality of BECCAL as laid out in Sect. 2 and 3.2. Each of these light paths must be controlled in terms of power, frequency, and polarization, as well as having dynamic control on suitable timescales.

The choice of elements has been motivated in Sect. 3.2.2. Additionally, in the context of the laser system, the  $D_2$  transitions of Rb and K at 780 nm and 767 nm, respectively, are easily accessible and have compatible natural linewidths with the light emitted by diode lasers [132].

The required light specifications are summarized in Table 1 and described below.

In Sect. 3.2.2 the MOT arrangement was described in terms of the physics package. In order to facilitate this, the laser system provides four light paths for the  $2D^+$ -MOT: two MOT beams, a pushing beam, and a retarding beam. In each of these paths, cooling and repumping light for both potassium and rubidium are overlapped. For the 3D-MOT, again four paths are provided for MOT beams with all four necessary frequency components overlapped in each fiber. It is possible to detune the light frequency by up to approximately  $\pm 200$  MHz from the cooling and repumping transitions. In addition to producing

**Table 1** Overview of the light fields delivered to the physics package from the laser system. The given power values correspond to the total power per set of fibers. All power values are estimates of the required and achievable powers rather than a guarantee of the power delivered

Function	Number of connections	Wavelength (nm)	Power (mW)	
			Cool	Repump
Detection	2	780	6	2
		767	7	7
3D-MOT	4	780	90	12
		767	75	65
2D-MOT	4	780	80	40
		767	70	70
Interferometry 1	1	780	15	15
		767	15	15
Interferometry 2	2	780	70	70
		767	70	70
Dipole trap	2	1064		300
Blue box	2	<767		50

a 3D-MOT, these beams will be used for sub-Doppler cooling prior to evaporation, thus necessitating the ability to smoothly ramp both frequency and intensity in these paths.

Two dipole trap paths at 1064 nm are provided for optical evaporation and other techniques such as DKC.

As outlined in Sect. 3.2.4, BECCAL will have two independent atom interferometry axes with light driving Raman transitions. Three separate paths deliver light to the two interferometry axes. One fiber will provide light for the primary interferometry axis. For the second interferometry axis, two individual paths are provided, as single Raman diffraction is to be realized on that axis. In the primary axis, two frequency components per species are overlapped in the fiber, whereas for the secondary axis, one component per species is used per fiber. The two different frequency components per species have a relative detuning equal to the ground state hyperfine splitting of the relevant isotope plus the two-photon recoil frequency and a variable detuning.

Two detection paths are provided for the techniques discussed in Sect. 3.2.6. Each of these paths have nominally the same power of all four frequency components. These light paths will also be used to provide light pulses suitable for quantum optics and information experiments and as such it will be possible to have a single frequency of light per fiber, with a different frequency component in each fiber.

The final two light paths provide the light required for blue-detuned dipole potentials. This light will have a wavelength below 767 nm.

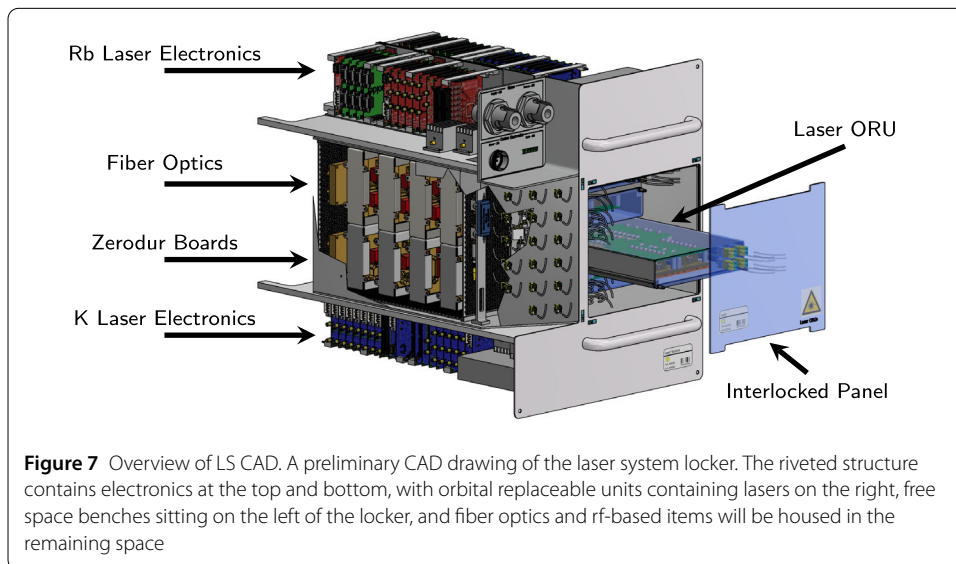
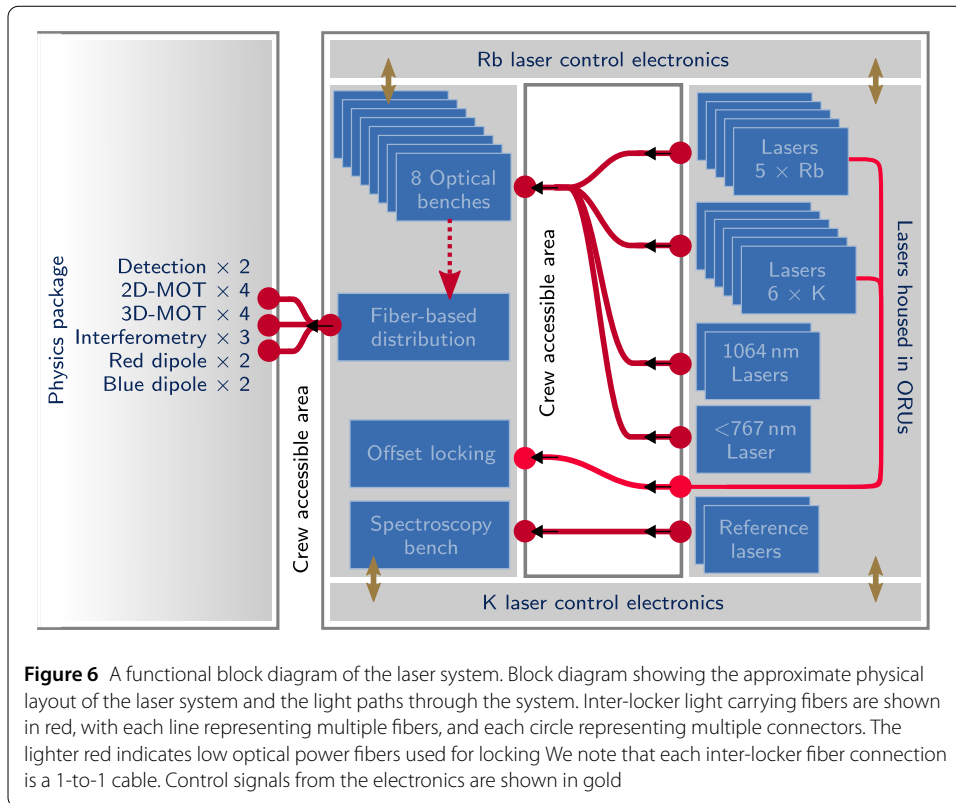
All lasers except those used for dipole potentials (both  $< 767$  nm and 1064 nm) must be locked to an atomic reference transition. We are able to use either modulation transfer spectroscopy (MTS) or frequency modulation spectroscopy (FMS) to lock two reference lasers – one locked to a transition in K and the other to a transition in Rb. All remaining lasers are offset-locked to the two reference lasers. Further details of this scheme can be found in Sect. 3.3.4.

Dynamic control of optical power will be implemented with three possible regimes: fast switching times of less than 10  $\mu$ s to  $-30$  dB, slower complete extinction in less than 10 ms, and linear modification across the dynamic range in 1 ms. This applies to all light paths delivered to the physics package except the interferometry beams, for which fast switching must be possible in less than 1  $\mu$ s. Optical power will be stabilized and measured before each experimental run.

### 3.3.2 Laser system architecture

The laser system is organized into three subsystems: lasers, free-space distribution, and fiber-based distribution. A functional block diagram showing these subsystems is shown in Fig. 6.

To deliver the optical powers shown in Table 1, a total of sixteen lasers are used. Six lasers emit light with a wavelength of 780 nm to address Rb (including one reference laser), seven lasers emit light with 767 nm to address K (including one reference laser), two lasers for the creation of red-detuned dipole traps at 1064 nm, and one laser runs at a wavelength below 767 nm for blue-detuned optical potentials. The light is created within an extended cavity diode laser master oscillator power amplifiers (ECDL-MOPA) configuration. Further details of these lasers are given in Sect. 3.3.3. They are shown on the right hand side of Fig. 6. The sixteen lasers will be housed in four removable boxes of four lasers each which are called orbital replaceable units (ORUs) (see Fig. 7). This ORU based approach is taken



as a form of redundancy such that a subset of lasers can be swapped out of the payload with minimal disturbance in the event of degradation.

The constraints set by the SWaP budget (Sect. 3.1.1) and the complexity of the experiment favor the use of free-space optics rather than fiber-based optical components. We integrate optics on ultra-stable optical benches made of Zerodur. These boards are presented in Sect. 3.3.4. This technology is also used in the form of a spectroscopy bench in order to lock our lasers to an atomic reference.

Many of the components of the laser system have been qualified through their use in sounding rocket and drop tower missions [29–31, 133–135]. For example, the current generation of laser modules flew in the JOKARUS mission [29, 30]. Furthermore, similar laser modules, Zerodur-based optical benches and commercial fiber-based components flew in MAIUS-1 [133], FOKUS [135] and KALEXUS [31]. In addition to flight-based qualification, ground based testing as well as vibration and shock tests have been carried out on components [136–138].

The safety requirements of the ISS (as described in Sect. 3.1.2) are of particular relevance to the laser system. As a result, the laser system is entirely inaccessible to the crew with the exception of the interface between the laser system and the physics package (seventeen optical connections), and between the laser ORUs and the rest of the laser system (up to thirty-two optical connections). Both sections are protected by interlocked panels.

Due to the large number of optical connections to be crew-made, it is necessary to choose fiber connectors which are both intuitive to use and robust over multiple mating cycles. The fiber connections from the laser system to the physics package will be made during installation, whereas the ORU connections will be made prior to flight (or by crew in the event of replacement). Each optical connection involves an optical fiber patch cord in a crew-accessible part of the payload and two mating sleeves (interfacing with the internal parts of the payload).

In order to ensure minimal optical losses, maximal polarization stability, and ease of use, *E2000* connectors and mating sleeves are being tested in a laboratory environment and the necessary additional qualification tests are planned.

### 3.3.3 Lasers

As laser sources, semiconductor diode lasers are ideal candidates for BECCAL: they are compact, robust, available in a variety of wavelengths and expected to be resilient against the thermo-mechanical loads associated with launch and operation conditions in BECCAL [136, 137, 139, 140]. To this end, micro-integrated laser modules will be used within BECCAL, as in heritage missions [29–31, 133, 134]. The laser modules are designed for versatility and multi-functionality through a design which incorporates two semiconductor-based active or passive chips and two optical ports that can be used as input or output ports. For instance, a master-oscillator power-amplifier (MOPA) architecture can be implemented, with the master-oscillator consisting of either a monolithic diode laser chip, such as a distributed feedback laser, or as in the case of BECCAL, a discrete ECDL, thus creating an ECDL-MOPA. The laser chips are micro-integrated onto a micro-optical bench consisting of lithographically patterned aluminium nitride (AlN) substrates together with micro-optics and discrete (as opposed to integrated) electronics components. A CAD model of a MOPA with an ECDL as master-oscillator is shown in Fig. 8a.

The micro-optical bench is fully packaged into a housing made of Kovar, which is a commercial available nickel–cobalt ferrous alloy. The electrical signals are fed through via Mini-SMP coaxial connectors and the optical signals are fed through via single mode, polarization-maintaining optical fibers. In the ECDL-MOPA configuration, two optical output ports are available – a main port that delivers the laser power to the physics package, and an auxiliary port, that can be used for the generation of beat notes or for monitoring purposes. The module housing has dimensions of 125 mm × 75 mm × 22.5 mm

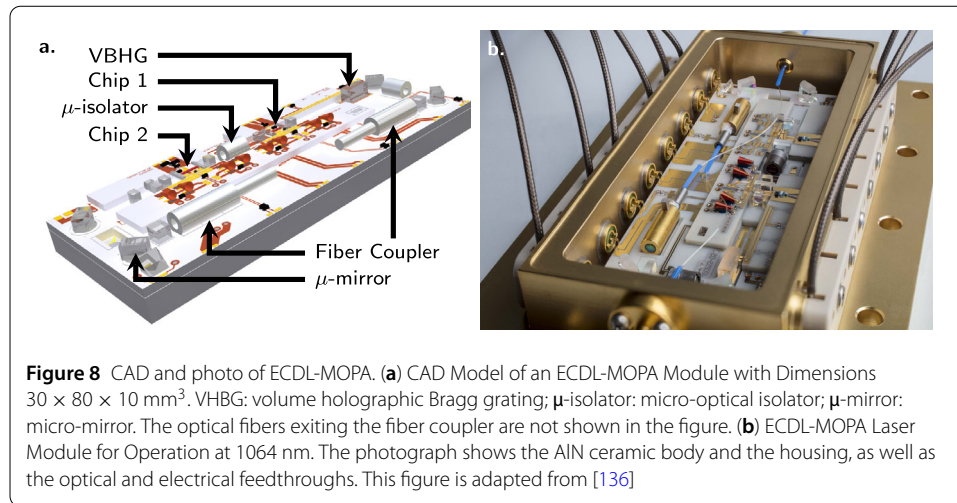


**Table 2** Main electro-optical expectations of the laser sources. PER: polarization Extinction Ratio; SMSR: Side Mode Suppression Ratio; FWHM: Full Width at Half Maximum

Functionality	Rb	K	Red-detuned dipole trap	Blue-detuned dipole trap
Central wavelength (nm)	780.241	766.701	1054 to 1074	<767
Output power (mW)	300	250	500	200
PER (dB)	-15	-15	-15	-15
SMSR (dBc)	30	30	30	30
linewidth (FWHM, 1 ms) (kHz)	100	100	100	100

and a mass of approximately 760 g. Figure 8b shows a picture of an ECDL-MOPA laser module. Such a laser module operating at a wavelength around 1064 nm [141] has successfully been flown as part of an iodine-based frequency reference in the JOKARUS mission [29, 30] on the TEXUS 54 sounding rocket in May 2018. It delivered more than 500 mW output power ex-fiber within a technical (FWHM) linewidth of 25 kHz measured on a timescale of 1 ms (estimated from the frequency noise power-spectral density according to the method proposed in [142]) and a Lorentzian linewidth of smaller than 1 kHz. The ECDL-MOPA technology has already been transferred to the wavelength of 780 nm for Rb-based experiments, such as MAIUS-B. At an emission wavelength of 780.24 nm (corresponding to the Rb  $D_2$  line), an optical output power of the ECDL-MOPA of  $\geq 400$  mW has been demonstrated. Identical diode laser chips and micro-optics technologies can be used to produce the ECDL-MOPAs emitting at 767 nm and for the blue-detuned optical trap. The expected performance of the lasers is shown in Table 2.

### 3.3.4 Free-space optics

As outlined previously, the majority of light control is performed via free-space optics. However, the conditions during a rocket launch and aboard the ISS necessitate a light distribution system of very high thermal and mechanical stability as well as small size. In order to meet these requirements, we utilize a range of miniaturized optical benches based on a toolkit first introduced in [143]. This technology has successfully been used in previous sounding rocket missions [31, 133, 135] and is going to be utilized within the MAIUS-2/3 missions [115, 138].

The foundations of this toolkit are optical benches made from Zerodur, a glass ceramic produced and manufactured by Schott AG. This material has a near zero coefficient of thermal expansion and mechanical properties similar to those of aluminium. Onto these optical benches, free-space optical components such as mirrors, beam splitters, etc. are glued. By using the appropriate components, any functionality that can be achieved with a laboratory based optical setup can also be realized using these benches.

A total of ten optical benches will be used for BECCAL. Eight of those benches will be used for light distribution and preparation, and the remaining two as spectroscopy benches. A rendering of one of the optical benches used for light distribution can be seen in Fig. 9a: In a first step, the light from a fiber is collimated using a fiber collimator (1). The light then passes an optical isolator (2) to suppress back-reflections into the laser. Most experimental sequences require intensity control and fast switching. To achieve this, we use a conjunction of an AOM (3) for fast suppression and a shutter (4) for complete suppression. Mirrors (6) are used to redirect the beam, and mirrors (5) angled at  $45^\circ$  with respect

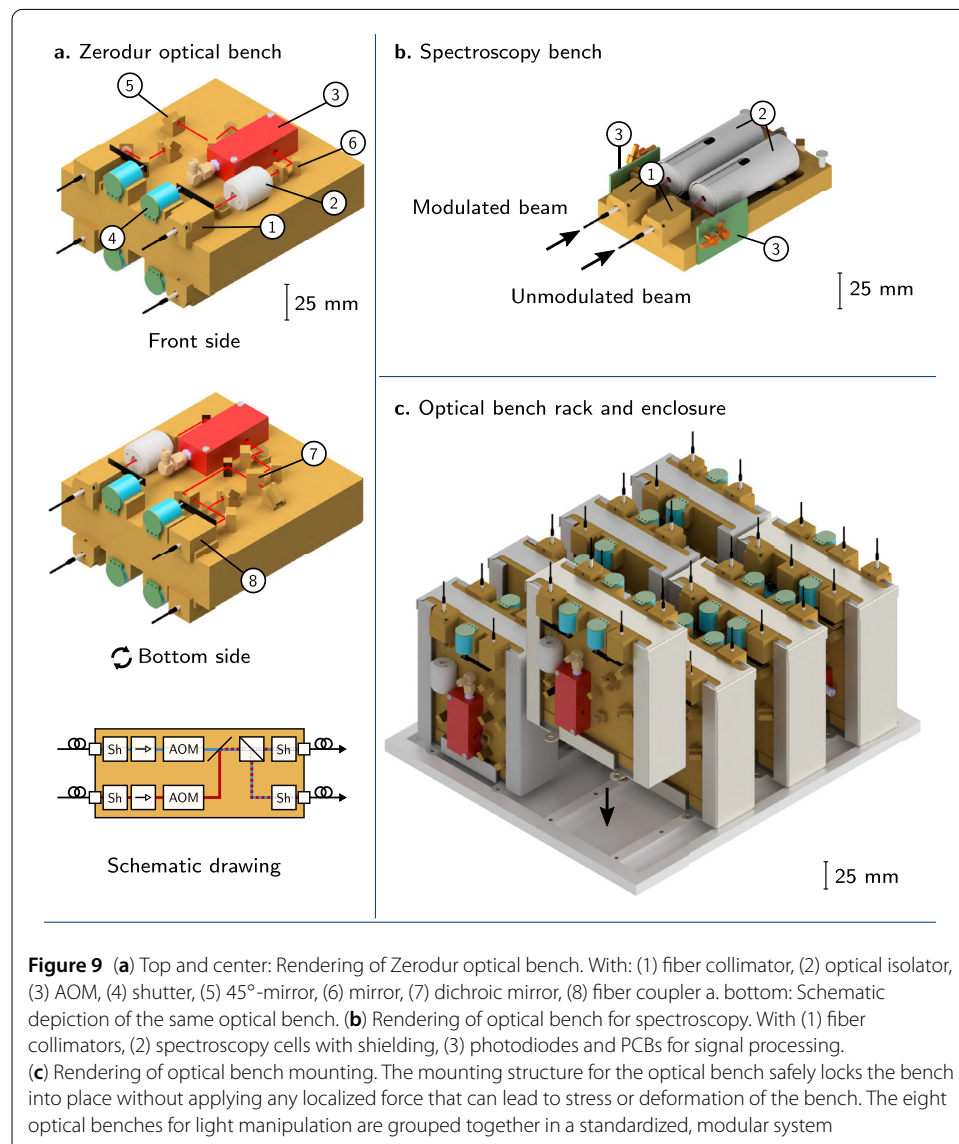


**Figure 9** (a) Top and center: Rendering of Zerodur optical bench. With: (1) fiber collimator, (2) optical isolator, (3) AOM, (4) shutter, (5)  $45^\circ$ -mirror, (6) mirror, (7) dichroic mirror, (8) fiber coupler a. bottom: Schematic depiction of the same optical bench. (b) Rendering of optical bench for spectroscopy. With (1) fiber collimators, (2) spectroscopy cells with shielding, (3) photodiodes and PCBs for signal processing. (c) Rendering of optical bench mounting. The mounting structure for the optical bench safely locks the bench into place without applying any localized force that can lead to stress or deformation of the bench. The eight optical benches for light manipulation are grouped together in a standardized, modular system

to the bench guide light through a hole in the optical bench to the opposite side. Using these, we can use both sides of the optical bench, thereby effectively doubling the usable surface as compared to single-sided benches. A dichroic mirror (7) is used to overlap the beams at 767 nm and 780 nm in the same polarization state. We split a beam into two beams by using waveplates and polarizing beam splitters. The light is then coupled back into a fiber using a fiber-coupler (8). We regularly achieve high fiber-coupling efficiencies of about 81% [143].

To match the stringent size and mass constraints aboard the ISS and to further improve stability, we have adapted and improved the above toolkit as follows [144]: The benches are mounted in a clamp-like support structure that holds the bench from all sides (see Fig. 9c). Between the bench and the support, a rubber material is used as a cushion to dampen vibrations and mediate any direct force that could result in coupling-losses. The eight distribution benches are aggregated into a mounting structure as shown in Fig. 9c. This modular system uses a standardized optical bench form factor with 30 mm thickness, 125 mm length and 100 mm or 120 mm width. This enables easy exchange of benches on ground during implementation.

For frequency stabilization of the lasers, two spectroscopy modules are being used. A rendering can be seen in Fig. 9b: Two light beams, one modulated, one unmodulated, are coupled onto a bench using two fiber couplers (1). They then counter-propagate through two spectroscopy cells (2), filled with the relevant atomic gas. After passing the cells, the modulated and unmodulated beam are then each redirected onto a fast photodiode, the signal of which is further processed on a PCB (3).

### 3.3.5 Fiber-based optics

Before and after the free-space optical benches, light is controlled and manipulated in a fiber optic system. The fiber optic system comprises of fiber splitting/overlapping, switches, in-line photodiodes and optical modulators.

Several arrays of fiber splitters are used both to split single outputs of the free-space benches or lasers, and for combining multiple light paths. Fiber splitters are used in places where symmetric splitting is required.

Fiber switches will be used both in the detection and interferometry paths to provide the flexibility needed within the system. Additionally to the switching capabilities provided by the AOMs and mechanical shutters included on the Zerodur free-space optical benches, the fiber switches also provide simultaneous extinction of multiple frequency components.

Radio-frequency-based fiber optics are used in the form of electro-optical modulators (EOMs) and one AOM. Two EOMs add frequency side-bands needed for spectroscopy. The AOM controls the intensity of the light for the first interferometry axis up to an extinction of  $-30$  dB.

In-line photodiodes will be an essential part of the BECCAL monitoring concept. A large amount of house-keeping and control data will be taken to monitor and characterize the performance of the system during its lifetime. Optical taps (of typical ratio 99:1) provide an efficient way to monitor optical powers across the payload and provide both housekeeping and troubleshooting data if necessary.

### 3.4 Control electronics

The control electronics system is the backbone of BECCAL, as it is in all quantum mechanics experiment. All active elements in BECCAL, which excludes metal parts and structural elements, are powered and controlled by the electronics presented in the following section. The whole BECCAL apparatus will have approximately 1.5 m<sup>2</sup> of circuit board, the majority of which is custom designed.

#### 3.4.1 Power budget

The power budget is governed by four main states: cold and hot standby, capacitor charging mode, and standard operational mode. In cold standby, all non-vital components are turned off and only the vacuum pumps, the communication and the monitoring stay on. In this mode, the apparatus draws 144 W of power. In hot standby, the system thermalizes prior to full operation mode. Here the laser system is switched on, with the rest of the apparatus in the same state as cold-standby. This mode results in 1066 W power consumption. In capacitor charging mode, the peak power increases to 1467 W. The peak power takes into account the maximum magnetic field of 175 G and all other systems in full operation. During the actual operation of the experiment, the power consumption drops back to the 1066 W of the hot standby mode because the chip and coil current drivers are supplied from capacitors and not from the 28 V line. In the standard operational mode, the apparatus alternates between charging the capacitors and running the experimental sequences. On average it will draw 1267 W of power, which directly translates into heat that needs to be dissipated. More detailed information on the distribution of the electrical power between the lockers can be found in Table 3. These numbers represent a worst case with every device powered-up. Depending on the actual experiment sequence, the real power will be lower, as unused parts can be powered down.

Due to the use of capacitors to store energy, the peak electrical power and the peak heat dissipation do not occur at the same time. Due to the cycle times of the experiments of typically a few seconds, the average power drives the thermal design (Sect. 3.1.1). The electronic design, however, is driven by the peak electrical power. Table 4 contains more detailed information on the heat dissipation per locker.

The electric power is drawn from four 28 V-EXPRESS Rack power outlets as each one is individually limited to 20 A at nominal 28 V [111]. This divides BECCAL logically in four groups: control electronics, chip&coil current drivers and the rubidium and potassium laser electronics. There is no power sharing between those groups. The power supply of the titanium sublimation pump is part of the chip&coil current driver group. In order

**Table 3** Electrical input power per wall plug: control electronics (CE), chip&coil current and titanium sublimation pump (CCC/TSP), rubidium laser system (LS-Rb), and potassium laser system (LS-K). Due to the usage of capacitors, the electrical peak power consumption does not occur in the same experimental phase as the peak heat dissipation listed in tab. 4

State (W)	CE (W)	CCC/TSP (W)	LS-Rb (W)	LS-K (W)	Total power (W)
Cold standby	144	0	0	0	144
Hot standby	324	84	318	340	1066
Capacitor charging	324	485	318	340	1467
Experiment operation	324	84	318	340	1066
Avg. charging + operation	324	285	318	340	1267
Ti-sublimation pump	144	372	0	0	516



**Table 4** Heat dissipation per locker: control electronics (CE), physics package (PP), and laser system (LS). Due to the usage of capacitors, the electrical peak power consumption, shown in tab. 3, does not occur in the same experimental phase as the peak heat dissipation

State	CE (W)	PP (W)	LS (W)	Total heat (W)
Cold standby	123	21	0	144
Hot standby	331	77	658	1066
Capacitor charging	367	77	658	1102
Experiment operation	586	187	658	1431
Avg. charging + operation	477	132	658	1267
Ti-sublimation pump	123	393	0	516

not to trip the circuit breaker of the EXPRESS rack, there are additional electronic circuit breakers in BECCAL.

### 3.4.2 Current drivers

In order to ensure the lowest possible noise for currents through the coils and the atom chip, the corresponding current drivers are powered by supercapacitors with output voltages between 5 V and 48 V. The current drivers themselves use a linear design to avoid switching noise. There will be separate electronic circuit breakers to protect the atom chip against faults in the current drivers.

The laser current drivers also use a linear design, with additional filtering in order to suppress power supply noise.

### 3.4.3 Experimental control, timing and data storage

All frequency and timing related signals are phase locked to a central oven-controlled crystal oscillator (OCXO). This ensures that the timing of all events are synchronized and all frequencies are as precise as the central reference. There will be a slow tracking of the OCXO frequency against GPS via the network time service of the ISS for post-corrections. All RF signal generators are direct digital synthesizers (DDS) based and generate signals in the range of 0.3 MHz to 150 MHz with a frequency resolution better than 0.1 Hz and will be capable of ramps and jumps in frequency, phase, and amplitude simultaneously. The microwave generators operate between 250 MHz and 6.8 GHz and are phase locked to DDS signal generators.

The main computer that controls the experiment will have a dual core Intel I7 processor with 8 GB RAM and 500 GB of non-volatile storage on two internal SSDs and another 500 GB on two external SSDs for experimental data.

The computer communicates to the ISS-Network and to the internal network via Ethernet. The internal network is based around a custom protocol on plastic optical fibers (POF), combining data, frequency, and trigger signals in a single wire pair, saving a lot of weight and space while at the same time avoiding ground loops.

## 3.5 Software operation

BECCAL's operation will be conducted in collaboration with scientists from many different institutions. The main goal is to enable all participants to have their experiments executed on the BECCAL instrument. This requires a robust structure and an easy-to-use software interface for the scientists.

For successful operation, four main software tools have been identified: the Experiment Control Software, the Experiment Design Tools, the Lab Operation Software, and the

Ground Control Software. All of the mentioned software tools use model-driven software technologies to either support users with the creation of valid experiment definitions, or to generate source code from engineering data of the experiment hardware.

### 3.5.1 *Experiment control software*

The Experiment Control Software is the software running on the on-board computer of the experiment. It communicates directly with the experiment electronics and is in charge of executing the experiment step by step. It is controlled through the Lab Operation Software or the Ground Control Software depending if it runs on one of the test beds or the BECCAL instrument on-board the ISS. The drivers for the control electronics described in Sect. 3.4 are largely generated from a model description. The capabilities of every electronic card and the stack it resides in are captured using domain specific languages [145]. Those descriptions serve as an unambiguous single point of truth and provide an interface between the electronic and software development domain. Changes in the firmware of an electronics card can then be reflected in the Experiment Control Software with very little manual effort which saves resources during the development of an experimental setup such as BECCAL.

The core elements for experiment execution are sequences and subsequences. Each sequence captures the next actions for the electronics in a precisely timed schedule in order to manipulate the state of the experiment. Frequently occurring actions can be placed in a subsequence, sharing common actions among sequences and avoiding code duplication.

A set of sequences is then assembled into sequence graphs, which, besides serial execution, also provides mechanisms to direct the experiment flow [145]. In this way the experiment can, for example, run through certain sequences multiple times with different input parameters and tune the experiment before entering into the next phase without the manual interaction of an operator.

This general separation between sequences and experiment-execution graph has already been used for the MAIUS-1 mission [28]. There, from the graphs, sequences, and subsequences, the corresponding C++ code was generated and compiled as part of the Experiment Control Software. For BECCAL this approach is not feasible as a wider range of experiments needs to be supported in a transparent and efficient way. Therefore, the graphs are stored as separate files. The Experiment Control Software for BECCAL includes a newly developed graph-interpret engine which interprets and executes the graphs directly from those files after successful sanity checks have been carried out. To ensure safety of the experiment at all times only graphs which have been previously qualified on a ground test bench will be uploaded to the ISS through the ground-control station. After experiment execution the full set of captured scientific data is stored on the on-board computer's hard drive and has to be downloaded before it can be distributed to the author of the experiment.

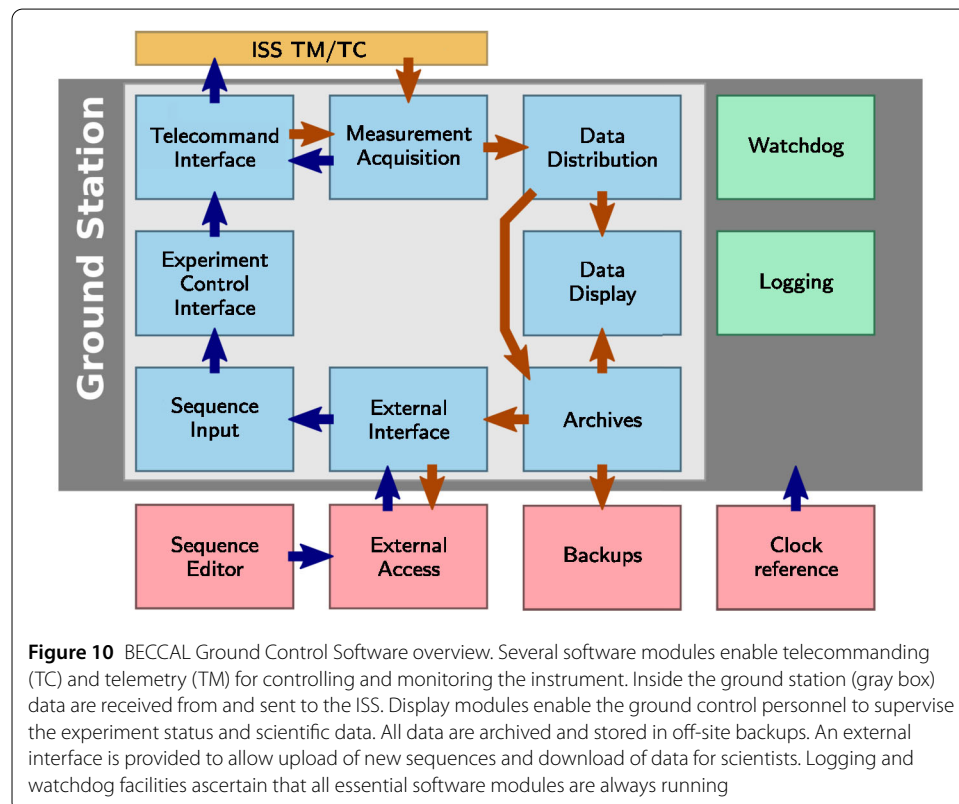
### 3.5.2 *Experiment design tools*

The Experiment Design Tools are the software components for the participating scientists in order to create a fully functional experiment. They support the scientists with the task of creating a formally correct experiment which can then be tested on one of the ground-based testbeds and later be qualified for the execution on board the ISS. For this purpose, the sequences and subsequences, as well as the graphs, are also created using a model

representation in the background. To this end domain specific languages were developed which describe sequences and subsequences in a human- and machine-readable textual representation, allowing for easy integration into version control systems. Graphical user interfaces (GUIs) allow experimenters to create and edit these sequences, as well as the graphs, in a convenient way. Both interfaces facilitate complex validation procedures using the model description of the hardware to indicate errors and potential problems to the user via visual markers. This model-driven approach also restricts the allowed features for the scientist to a set which is qualifiable for the execution on board the ISS.

### 3.5.3 Ground control software

The Ground Control Software is the single point of communication to the BECCAL instrument on board of the ISS during normal operation. It comprises several software modules, which are depicted in Fig. 10. A telecommand interface provides means to control the experiments, while a telemetry interface receives live housekeeping data at all times and scientific data during operation. Custom protocols for telecommands and telemetries will be used alongside standard tools such as *ssh* and *rsync* for maintenance and file transfers. Data is distributed by the telemetry module via network to display modules for operators to supervise operation and to a central archive, which is copied to one or more off-site backups. In the archive and the backups, redundant file systems with checksumming-capabilities will ensure data integrity. From there, a web interface allows scientists to access data of their experiments. The same interface will allow scientists to upload new experimental sequences and graphs, which are then validated and uploaded to the Experiment Control Software. A logging service keeps track of all events and inputs for debugging



purposes, and a watchdog services ensures that all critical software modules, are running at all times.

The most important objective is the safe operation of the instrument at all times. Therefore, only qualified sequences and graphs are allowed to be uploaded to and executed on the instrument. The Ground Control Software is responsible for ensuring data integrity of the uploaded data before execution. It also collects and monitors BECCAL's telemetry data and executes standard maintenance tasks. If non-nominal telemetry is received, the Ground Control Software is also capable of aborting ongoing experiments if necessary, and bringing the instrument back in a nominal state. After an experiment execution is finished, the system initializes the download of all generated scientific data from the experiment which can subsequently be distributed to the responsible scientists.

#### *3.5.4 Lab operation software*

The Lab operation software is responsible for communication with the Experiment Control Software (ECS) in the laboratory environment of the testbed. It commands the ECS to execute graphs or sequences and presents the received live telemetry data. Essentially, it extends the Ground Control Software to facilitate a more direct interaction with the ECS, allowing, for example, the execution of not yet qualified sequences or graphs. This enables the operators to debug or optimize parts of an experiment. The Lab operation software operates on the same model representation as generated by the Experiment Design Tools, anomalies which occur during execution can therefore directly be discussed with the author of the experiment with the same unambiguous input data.

## **4 Operations**

BECCAL will be installed in the US Destiny module on board the ISS. Operations include the delivery to the launch site, launch, installation in orbit, check-out procedures, operations, data distribution, proprietary rights, removal from orbit, and post-flight operations.

### **4.1 Launch**

After integration in Germany, the payload is delivered to the designated launch site, where it is integrated into the transport capsule. At the time of writing, the exact launcher has not been confirmed, and as such, details of related operations and requirements will be decided upon once the launch vehicle is known. The current design allows for transport with any of the currently available launchers.

Independent of the exact launcher, the experiment is expected to be exposed to vibrations of 8.8  $g_{\text{rms}}$  and shocks of up to 12 g during launch. Therefore the hardware must be tested prior to flight to ensure it is able to withstand the expected launch.

### **4.2 Installation and check-out**

On arrival in orbit, the payload will be installed by the crew, which includes establishing interfaces to the ISS and between lockers. Installation is completed with the initial power-up of the payload which is done by both the crew in orbit and the crew on ground.

After installation, BECCAL will undergo a series of test procedures to assure operation readiness and to verify remaining requirements (such as those only achievable in micro-gravity). This process includes the check of the health and status data as well as the execution of the first experimental sequences.

### 4.3 On-orbit operation

Following successful payload check-out, BECCAL will go into nominal operation. In nominal operation, BECCAL will execute experimental sequences, which are prepared on ground and tested using a ground testbed.

During operation, the experiment will be controlled and monitored via a datalink from ground (Sect. 3.5). The quiet times onboard the ISS are preferred for operation to avoid disturbances by excess vibrations due to astronaut activities.

The operation of BECCAL is divided into three parts: cold standby, hot standby, and experimental operation. The later one can be further divided into charging and experimental phases. Technical details are discussed in Sect. 3.4

*Cold standby* During cold standby, all non-vital components are off. Such that the ion getter pump is operational, and the payload computer records health and status data.

*Hot standby* Approximately thirty to sixty minutes prior to experimental operation, the payload is set into hot standby. During hot standby the subsystems are prepared for experimental operation. In particular, this includes the thermalization of the laser system. After experimental operation, the system is kept in hot standby for performance checks before it is sent to cold standby.

*Experimental operation* Experimental operation is divided into charging and experimental phases. During the experimental phase, the pre-programmed and tested sequences are executed. The two phases are of roughly equal duration.

The duration of experimental operation is based on the rhythm of the crew on board and the available resources both on ground and in orbit.

### 4.4 Performing an experiment on BECCAL

The process of performing an experiment on BECCAL has several stages:

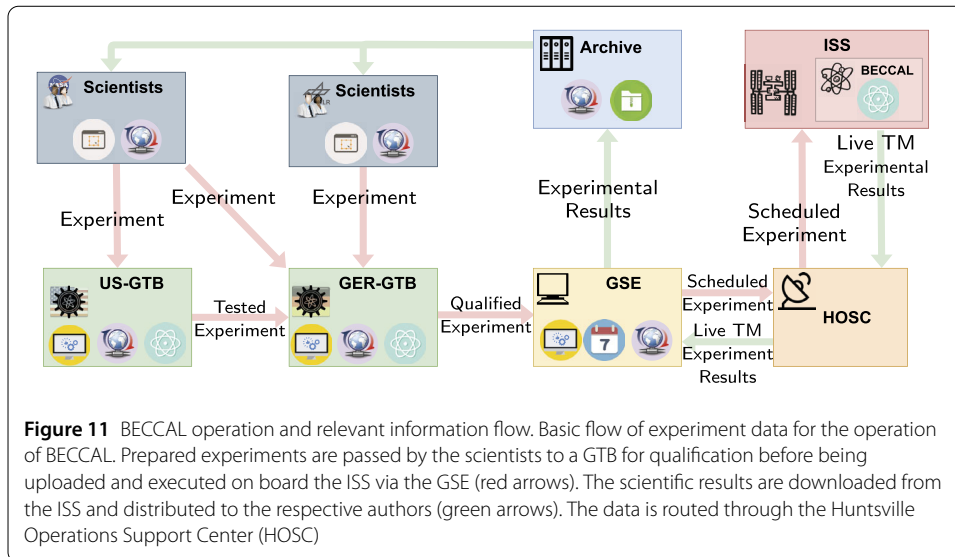
First, the defined experiments are translated into executable sequences. These then undergo both software based and testbed based checking to ensure suitability for execution on BECCAL. The software checks for formal conformity, whilst the testbed operators are able to review the designed experiment sequences for errors, execute them on the testbed, return the experimental results, and suggest adaptations to improve the sequences.

If the experimental sequence is deemed ready for execution on BECCAL, it is sent to the German ground-based testbed for final qualification. To ensure that the sequence can be executed on the flight hardware, it must always be qualified on the German ground-based testbed, which is similar to the flight system and runs both the ground control software and the current version of the experiment control software.

Once a sequence is successfully qualified no further changes are possible without re-qualification.

The qualified experimental sequence is finally forwarded to the BECCAL ground-control station and scheduled for on-board operation. Upon download of the experiment's scientific data set, the results are distributed.

Figure 11 presents a high-level overview of the different stages and the information flow in between.



#### 4.5 Network communications

Communication between the Ground Control Station and the instrument are handled via standard IP based network protocols. A bidirectional transparent network link can be established between the Ground Control Station and the onboard computer, which runs the Experiment Control Software.

Live telemetry of essential housekeeping data is sent to ground in UDP packets to allow monitoring of the instrument's status from the Ground Control Station. Complete data sets can reach several Gigabytes in size and are thus buffered on the onboard computer and downlinked during standby via file-transfer protocols which ensure data integrity.

In the Ground Control Station, data are archived and migrated to systems which enable access for scientists to their respective data sets.

#### 4.6 Maintenance

BECCAL will make use of orbital replaceable units in order to provide some degree of redundancy in case of an error that cannot be resolved from ground. In such cases, each enclosed locker structure (laser system, physics package, control electronics) can be exchanged with a replica system already assembled and tested on ground. Additionally, the lasers modules are themselves housed in smaller ORUs such that they can be replaced without replacing the entire laser locker as discussed in Sect. 3.3.

#### 4.7 Lifetime and de-commissioning

BECCAL shall be operational for a minimum of twelve months and is intended to be installed in orbit for three years.

After the in-orbit period of three years, the condition of the payload and the available resources will be assessed before BECCAL is de-integrated. It is not planned for the hardware to be returned to ground.

### 5 Summary of experimental capabilities

BECCAL is expected to offer a high flux of ultracold rubidium and potassium gases. These gases can be brought to quantum degeneracy in less than 2 s, supporting experiments that

require extensive statistics. The magnetic fields are generated by a multi-layer atom chip, with a design similar to the ones used in QUANTUS [23] and MAIUS [28], in combination with four pairs of coils, three of which are oriented perpendicular to each other. The fourth pair of coils produces a large magnetic field to tune the scattering length of the atoms. Additionally, the atoms can be manipulated with radio frequency and microwave fields. This setup allows the creation of adiabatic-dressed potentials for hollow BECs or the formation of an atom laser.

Furthermore, the atoms can be exposed to blue-detuned laser light from two perpendicular directions. These beams can be spatially controlled to create traps of arbitrary shapes in three dimensions. Red-detuned light can also be used for crossed dipole trapping or the creation of optical lattices.

The atom chip will have different areas with metallic coating for investigations of atom-surface effects. The detection is carried out by either capturing the fluorescence signal of the atoms or by taking spatially resolved absorption images. The absorption imaging systems will allow for changing the focal plane and the field of view.

Moreover, BECCAL will have two perpendicular atom interferometry axes. One axis is nadir pointing and so is in the direction of the gravitational acceleration. Since this configuration is prone to contrast losses due to the rotation of the ISS, the retro-reflection mirror is mounted on a piezo-tip-tilt stage inside the vacuum chamber. An overview of the core parameters is given in Table 5.

## 6 Conclusion

We have presented the current design of the BECCAL experiment, an apparatus intended to perform experiments with cold atoms and Bose-Einstein condensates in microgravity on board the ISS. It is a joint endeavor of DLR and NASA. The described design complies with constraints on size, mass and power as well as the stringent requirements on safety and robustness which are mandatory for accommodation and remote operation in a manned spacecraft. It builds upon the heritage of previous experiments performed in drop towers, sounding rockets, and the ISS.

BECCAL is conceived as a multi-user and multi-purpose facility and designed for broad range of scientific applications. BECCAL includes capabilities for magnetic traps, optical dipole traps, state preparation, coherent manipulation, and multiple detection systems. These capabilities, in combination with the atomic species choice of rubidium and potassium, will enable the generation of degenerate Bose-Bose as well as Bose-Fermi mixtures, the study of shell-shaped and uniform quantum gases, quantum reflection on surfaces, experiments on few-body physics, and atom interferometry with BECs and quantum gas mixtures. For all these experiments persistent microgravity is a crucial feature, either by actually enabling them or by greatly enhancing their performance, due to suppressing the gravitational sag and increasing free fall times beyond typical experiments on earth. We anticipate many exciting and fruitful additional ideas and topics for research in the frame of BECCAL above and beyond the carefully compiled list presented here. In conclusion, we expect BECCAL to advance the current understanding of fundamental physics in the field of quantum and atom optics as well as to advance the development of quantum sensors.

**Table 5** Overview of the experimental capabilities of BECCAL

<i>Atom numbers</i>	
Single $^{87}\text{Rb}$ BEC	$\geq 1 \times 10^6$
Single $^{41}\text{K}$ BEC	$\geq 1 \times 10^5$
Dual-species BEC of $^{87}\text{Rb}$ and $^{41}\text{K}$ (respectively)	$\geq 1 \times 10^5, \geq 1 \times 10^4$
Trapped $^{85}\text{Rb}$ atoms	$\geq 1 \times 10^6$
Trapped $^{39}\text{K}$ atoms	$\geq 1 \times 10^5$
Trapped $^{40}\text{K}$ atoms	$\geq 1 \times 10^4$
<i>Atom trapping and manipulation</i>	
Magnetic traps: available structures	Atom chip and four pairs of coils
Crossed optical dipole trap: wavelength, beam waist, total power	1064(10) nm, 100(20) $\mu\text{m}$ , 300 mW
Optical lattice	Switchable retro-reflection of the beams of the crossed optical dipole trap
Painted potentials: barrier height, sizes of rings, total power	5 $\mu\text{K}$ with contour length $\leq 100 \mu\text{m}$ and refresh rate $\geq 100$ Hz, inner diameter 20 $\mu\text{m}$ to 1500 $\mu\text{m}$ and outer diameter 40 $\mu\text{m}$ to 2000 $\mu\text{m}$ , 50 mW optical power at 764 nm
Life times of single species clouds: non-trapped, magnetically, and optically trapped (respectively)	$\geq 10$ s, $\geq 3$ s, $\geq 10$ s
Feshbach-field	$\geq 175$ G with tunable modulation of up to 1 G at $\geq 0.1$ kHz
Transport of atoms away from the chip	0.1 mm to 2 mm
Minimum expansion velocity for $^{87}\text{Rb}$ , $^{41}\text{K}$ , and $^{87}\text{Rb}$ - $^{41}\text{K}$ mixtures after atomic lensing	$\leq 100 \mu\text{m s}^{-1}$
Two independent radio-frequency sources	0.1 MHz to 25 MHz with Rabi frequency $\geq 10$ kHz and ramp rates $\geq 100 \text{ MHz s}^{-1}$
Microwave generator	6.835 GHz, 3.036 GHz, 1285 MHz, 462 MHz and 254 MHz adjustable with 30 MHz around the central frequency, Rabi frequency $\geq 10$ kHz and ramp rates $\geq 100 \text{ MHz s}^{-1}$
<i>Atom interferometry, two independent axes</i>	
Primary axis	parallel to Earth's acceleration (nadir) and parallel to the chip surface
Total free evolution time	$\geq 2T = 2.6$ s
Raman diffraction beams	splitting efficiency $\geq 90\%$ , $1/e^2$ beam diameter $\geq 6$ mm, Rabi frequency 1 kHz to 50 kHz, detuning adjustable 1 GHz to 5 GHz, homogeneous magnetic field of 0.05 G to 1 G, power of 15 mW (70 mW) per frequency component in primary axis (secondary axis)
Rotation compensation	retro-reflection mirror on tip-tilt stage for rotation compensation of ISS for times $\geq 2T = 2.6$ s ( $\geq 3$ mrad)
Coupling with external sensors	rotation sensor with noise floor $\leq 50 \mu\text{rad s}^{-1}/\sqrt{\text{Hz}}$
Secondary axis	perpendicular to the orbital plane and perpendicular to the chip surface
<i>Two orthogonal, species selective, spatially resolved absorption detection systems</i>	
Spatial resolution	$\leq 10 \mu\text{m}$
Field of view	$\geq 10 \text{ mm}^2$
Scanning range of focal plane	$\geq 10$ mm,
Adjustable depth of field	100 $\mu\text{m}$ to 2000 $\mu\text{m}$
Fluorescence detection	single axis, species selective
<i>Miscellaneous</i>	
Multiple surfaces with different electrical properties on the atom chip	size $\geq 1 \text{ mm}^2$



### Funding

The herein described project is a bilateral collaboration between NASA and DLR, both contributing to the scientific and operational organization. This work is supported by the German Space Agency (DLR) with funds provided by the Federal Ministry for Economic Affairs and Energy (BMWi) due to an enactment of the German Bundestag under Grant Nos. DLR50WP1431-1435, 50WM1131-1137, 50MW0940, 50WM1240, 50WM1556, 50WP1700-1706, 50WP1806, 50WP1836, 50WM1861, 50WM1955, 50WM1956, 50RK1957, 50WM2060, by "Niedersächsisches Vorab" through the "Quantum- and Nano-Metrology (QUANOMET)" initiative within the project QT3, through the Deutsche Forschungsgemeinschaft (DFG, German Research Foundation) under Germany's Excellence Strategy – EXC 2123 QuantumFrontiers, Project-ID 390837967, and through "Förderung von Wissenschaft und Technik in Forschung und Lehre" for the initial funding of research in the new DLR Institutes (DLR-SI and DLR-QT). MAE thanks the Center for Integrated Quantum Science and Technology (IQ<sup>ST</sup>) for financial support. The project was carried out in part at the Jet Propulsion Laboratory, California Institute of Technology, under a contract with the National Aeronautics and Space Administration (80NM0018D0004). The team acknowledges the contributions from NASA and their aid in adapting the payload to the needs of the International Space Station. We especially acknowledge the contributions from NASA Headquarters, Glenn Research Center, and Johnson Space Center. Open Access funding enabled and organized by Projekt DEAL.

### Abbreviations

AlN, Aluminium Nitride; AOD, Acousto-Optical Deflector; AOM, Acousto-Optical Modulator; BEC, Bose Einstein Condensate; BECCAL, Bose-Einstein Condensate and Cold Atom Laboratory; CAD, Computer-Aided Design; CAL, Cold Atom Laboratory; CCC, Chip Coil Current; CE, Control Electronics; DDS, Direct Digital Synthesizer; DKC, Delta-Kick Collimation; DLR, Deutsches Zentrum für Luft- und Raumfahrt; EXPRESS, EXpedite the Processing of Experiments to the Space Station; ECDL, External Cavity Diode Laser; ECS, Experiment Control Software; EOM, Electro-Optical Modulator; Fig, Figure; FMS, Frequency Modulation Spectroscopy; FOKUS, Faserlaserbasierter Optischer Kammgenerator unter Schwerelosigkeit; FWHM, Full Width Half Maximum; GER, German; GPS, Global Positioning System; GSE, Ground Support Equipment; GTB, Ground TestBed; GUI, Graphical User Interface; HOSC, Hunstville Operation Support Center; IGP, Ion Getter Pump; IP, Internet Protocol; ISS, International Space Station; JOKARUS, Jod Kamm Resonator unter Schwerelosigkeit; K, Potassium; KALEXUS, Kalium Laser-Experimente unter Schwerelosigkeit; LS, Laser System; MAIUS, Materiewellen-Interferometer unter Schwerelosigkeit; MOPA, Master Oscillator Power Amplifier; MOT, Magneto-Optical Trap; MTS, Modulation Transfer Spectroscopy; NASA, National Aeronautics and Space Administration; ORU, Orbital Replaceable Unit; PCB, Printed Circuit Board; PER, Polarization Extinction Ratio; POF, Plastic Optical Fiber; PP, Physics Package; OCOXO, Oven-Controlled-Crystal-Oscillator; QUANTUS, Quantengase unter Schwerelosigkeit; RAM, Random Access Memory; Rb, Rubidium; RF, Radio Frequency; RMS, Root Mean Square; Sec, Section; SMP, Sub-Miniature Push-on; SLM, Spatial Light Modulator; SMSR, Side Mode Suppression Ratio; SSD, Solid State Disk; SWaP, Size, Weight, and Power; Tab, Table; TC, Telecommanding; TM, Telemetry; TEXUS, Technologische Experimente unter Schwerelosigkeit; TSP, Titanium Sublimation Pump; UDP, User Datagram Protocol; UFF, Universality of Free Fall; VHBG, Volume Holographic Bragg Grating.

### Availability of data and materials

Not applicable.

### Competing interests

The authors declare that they have no competing interests.

### Authors' contributions

All authors contributed to the writing of the manuscript. The systems engineering, thermal design and simulation, mechanical and interface design as well as the design of the vacuum / pump system of BECCAL has been surveyed by a group led by JG and CB. The work of the group has been distributed among JP, MW, and JG. The laser subsystem has been led by VAH, with design work distributed between VAH (overall), AB (lasers), JPM, and AW (zerodur benches). The electronics are designed by TW and his group. KF, SvAb, DB, CS, and WH designed the physics package supported by PF for coils and the magnetic shield. TF, DL, HaM, AMN, ArP, and JS worked on the software. MAE, MaMe, AR, and WPS provided theory support with MaMe coordinating the effort. NY, JK, SWC, and UI worked on the development of the realization of the blue box potential. The members of the science definition team (SDT) DMSK, NL, HM (US-SDT) and WPS, EMR, DB, MK (GER-SDT) defined the scientific envelope. All authors read and approved the final manuscript.

### Author details

<sup>1</sup>Institut für Quantenoptik, Leibniz Universität Hannover, Welfengarten 1, D-30167 Hannover, Germany.

<sup>2</sup>Ferdinand-Braun-Institut, Leibniz-Institut für Höchstfrequenztechnik, Gustav-Kirchhoff-Str. 4, D-12489 Berlin, Germany.

<sup>3</sup>Institut für Mikroelektronische Systeme, Leibniz Universität Hannover, Appelstraße 4, D-30167 Hannover, Germany.

<sup>4</sup>ZARM, Universität Bremen, Am Fallturm 2, D-28359 Bremen, Germany. <sup>5</sup>German Aerospace Center for Space Systems, DLR-RY, Linzerstrasse 1, D-28359 Bremen, Germany. <sup>6</sup>Jet Propulsion Laboratory, California Institute of Technology, 4800 Oak Grove Drive, Pasadena, CA, 91109, USA. <sup>7</sup>Institut für Quantenphysik and Center for Integrated Quantum Science and Technology (IQST), Universität Ulm, Albert-Einstein-Allee 11, D-89069 Ulm, Germany. <sup>8</sup>Institute of Quantum Technologies, German Aerospace Center (DLR), Söflinger Str. 100, D-89077 Ulm, Germany. <sup>9</sup>Institute for Satellite Geodesy and Inertial Sensing, German Aerospace Center (DLR) c/o Leibniz Universität Hannover, Welfengarten 1, D-30167 Hannover, Germany. <sup>10</sup>Fierlinger Magnetics GmbH, Rathausplatz 2, D-85748 Garching, Germany. <sup>11</sup>Institute for Software Technology, German Aerospace Center (DLR), Lilienthalpl. 7, D-38108 Braunschweig, Germany. <sup>12</sup>AG Optical Metrology, Humboldt-Universität zu Berlin, Newtonstraße 15, D-12489 Berlin, Germany. <sup>13</sup>Institut für Laserphysik, Universität Hamburg, Luruper Chaussee 149, D-22761 Hamburg, Germany. <sup>14</sup>Institute for Satellite Geodesy and Inertial Sensing, German Aerospace Center (DLR) c/o Universität Bremen, Am Fallturm 9, D-28359 Bremen, Germany. <sup>15</sup>Department of Physics and Astronomy, Bates College, Lewiston, ME, 04240, USA. <sup>16</sup>Institut für Physik, Johannes Gutenberg-Universität Mainz, Staudingerweg 7, D-55128 Mainz, Germany. <sup>17</sup>Department of Physics, University of California, 366 LeConte Hall/UC 7300, Berkeley, CA, 94720-7300, USA. <sup>18</sup>Hagler Institute for Advanced Study and Department of Physics and Astronomy,

Institute for Quantum Science and Engineering (IQSE), Texas A&M AgriLife Research, Texas A&M University, College Station, TX, 77843-4242, USA. <sup>19</sup>Airbus Defence and Space, Willy-Messerschmitt-Straße 1, D-82024 Taufkirchen, Germany. <sup>20</sup>Space Dynamics Laboratory, Albuquerque, NM, 87106, USA.

## Publisher's Note

Springer Nature remains neutral with regard to jurisdictional claims in published maps and institutional affiliations.

Received: 13 May 2020 Accepted: 18 December 2020 Published online: 04 January 2021

## References

1. Foot CJ. Atomic physics. Oxford master series in physics. Oxford: Oxford University Press; 2005.
2. Berman PR. Atom interferometry. San Diego: Academic Press; 1997.
3. Gaunt AL, Schmidutz TF, Gotlibovych I, Smith RP, Hadzibabic Z. Bose-Einstein condensation of atoms in a uniform potential. *Phys Rev Lett*. 2013;110(20):1.
4. Sun K, Padavić K, Yang F, Vishveshwara S, Lannert C. Static and dynamic properties of shell-shaped condensates. *Phys Rev A*. 2018;98(1):013609.
5. Schlippert D, Hartwig J, Albers H, Richardson LL, Schubert C, Roura A et al. Quantum test of the universality of free fall. *Phys Rev Lett*. 2014;112(20):203002.
6. Berrada T, Van Frank S, Bücker R, Schumm T, Schaff JF, Schmiedmayer J. Integrated Mach-Zehnder interferometer for Bose-Einstein condensates. *Nat Commun*. 2013;4:1–8.
7. Leanhardt AE, Pasquini TA, Saba M, Schirotzek A, Shin Y, Kielpinski D et al. Cooling Bose-Einstein condensates below 500 picokelvin. *Science*. 2003;301(5639):1513–5.
8. Harber DM, Obrecht JM, McGuirk JM, Cornell EA. Measurement of the Casimir-Polder force through center-of-mass oscillations of a Bose-Einstein condensate. *Phys Rev A*. 2005;72(3):1.
9. Lundblad N, Carollo RA, Lannert C, Gold MJ, Jiang X, Paseltiner D et al. Shell potentials for microgravity Bose-Einstein condensates. *npj Microgravity*. 2019;5(1):30.
10. Kovachy T, Asenbaum P, Overstreet C, Donnelly CA, Dickerson SM, Sugarbaker A et al. Quantum superposition at the half-metre scale. *Nature*. 2015;528(7583):530–3.
11. Burrage C, Copeland EJ, Hinds EAA. Probing dark energy with atom interferometry. *J Cosmol Astropart Phys*. 2015;2015(03):042.
12. Jaffe M, Haslinger P, Xu V, Hamilton P, Upadhye A, Elder B et al. Testing sub-gravitational forces on atoms from a miniature in-vacuum source mass. *Nat Phys*. 2017;13(10):938–42.
13. Sabulsky DO, Dutta I, Hinds EA, Elder B, Burrage C, Copeland EJ. Experiment to detect dark energy forces using atom interferometry. *Phys Rev Lett*. 2019;123:061102.
14. Graham PW, Hogan JM, Kasevich MA, Rajendran S, Romani RW. Mid-band gravitational wave detection with precision atomic sensors. *arXiv*. 2017.
15. Tino GM, Bassi A, Bianco G, Bongs K, Bouyer P, Cacciapuoti L et al. SAGE: a proposal for a space atomic gravity explorer. *Eur Phys J D*. 2019;73(11):228.
16. El-Neaj YA, Alpigiani C, Amairi-Pyka S, Araújo H, Balaž A, Bassi A et al. AEDGE: atomic experiment for dark matter and gravity exploration in space. *EPJ Quantum Technol*. 2020;7(1):6.
17. Bidet Y, Zahzam N, Blanchard C, Bonnin A, Cadoret M, Bresson A et al. Absolute marine gravimetry with matter-wave interferometry. *Nat Commun*. 2018;9(1):627.
18. Barrett B, Bertoldi A, Bouyer P. Inertial quantum sensors using light and matter. *Phys Scr*. 2016;91(5):053006.
19. van Zoest T, Gaaloul N, Singh Y, Ahlers H, Herr W, Seidel ST et al. Bose-Einstein condensation in microgravity. *Science*. 2010;328(5985):1540–3.
20. Müntinga H, Ahlers H, Krutzik M, Wenzlawski A, Arnold S, Becker D et al. Interferometry with Bose-Einstein condensates in microgravity. *Phys Rev Lett*. 2013;110(9):093602.
21. Stern G, Battelier B, Geiger R, Varoquaux G, Villing A, Moron F et al. Light-pulse atom interferometry in microgravity. *Eur Phys J D*. 2009;53(3):353–7.
22. Langlois M, De Sarlo L, Holleville D, Dimarcq N, Schaff JF, Bernon S. Compact cold-atom clock for onboard timebase: tests in reduced gravity. *Phys Rev Appl*. 2018;10(6):064007.
23. Rudolph J, Herr W, Grzeschik C, Sterneke T, Grote A, Popp M et al. A high-flux BEC source for mobile atom interferometers. *New J Phys*. 2015;17(6):065001.
24. Vogt C, Woltmann M, Herrmann S, Lämmerzahl C, Albers H, Schlippert D et al. Evaporative cooling from an optical dipole trap in microgravity. *Phys Rev A*. 2020;101:013634.
25. Lotz C, Wessargues Y, Hermsdorf J, Ertmer W, Overmeyer L. Novel active driven drop tower facility for microgravity experiments investigating production technologies on the example of substrate-free additive manufacturing. *Adv Space Res*. 2018;61(8):1967–74.
26. Chiow S, Yu N. Multiloop atom interferometer measurements of chameleon dark energy in microgravity. *Phys Rev D*. 2018;97:044043.
27. Condon G, Rabault M, Barrett B, Chichet L, Arguel R, Eneriz-Imaz H et al. All-optical Bose-Einstein condensates in microgravity. *Phys Rev Lett*. 2019;123:240402.
28. Becker D, Lachmann MD, Seidel ST, Ahlers H, Dinkelaker AN, Grosse J et al. Space-borne Bose-Einstein condensation for precision interferometry. *Nature*. 2018;562(7727):391–5.
29. Schkolnik V, Döringshoff K, Gutsch FB, Oswald M, Schuldt T, Braxmaier C et al. JOKARUS - design of a compact optical iodine frequency reference for a sounding rocket mission. *EPJ Quantum Technol*. 2017;4(1):9.
30. Döringshoff K, Gutsch FB, Schkolnik V, Kürbis C, Oswald M, Pröbster B et al. Iodine frequency reference on a sounding rocket. *Phys Rev Appl*. 2019;11(5):1.
31. Dinkelaker AN, Schiemang M, Schkolnik V, Kenyon A, Lampmann K, Wenzlawski A et al. Autonomous frequency stabilization of two extended-cavity diode lasers at the potassium wavelength on a sounding rocket. *Appl Opt*. 2017;56(5):1388.

32. Elliott E, Krutzik M, Williams J, Thompson R, Aveline D. NASA's Cold Atom Lab (CAL): system development and ground test status. *npj Microgravity*. 2018;4(1):16.
33. Aveline DC, Williams JR, Elliott ER, Dutenhoffer C, Kellogg JR, Kohel JM et al. Observation of Bose–Einstein condensates in an Earth-orbiting research lab. *Nature*. 2020;582(7811):193–7.
34. Ammann H, Christensen N. Delta kick cooling: a new method for cooling atoms. *Phys Rev Lett*. 1997;78(2):2088–91.
35. Meister M, Roura A, Rasel EM, Schleich WP. The space atom laser: an isotropic source for ultra-cold atoms in microgravity. *New J Phys*. 2019;21(1):013039.
36. Barrett B, Antoni-Micollier L, Chichet L, Battelier B, Lévêque T, Landragin A et al. Dual matter-wave inertial sensors in weightlessness. *Nat Commun*. 2016;7:13786.
37. Hogan JM, Johnson DMS, Kasevich MA. Light-pulse atom interferometry. 2008. [arXiv:0806.3261](https://arxiv.org/abs/0806.3261).
38. Bongs K, Launay R, Kasevich MA. High-order inertial phase shifts for time-domain atom interferometers. *Appl Phys B*. 2006;84:599.
39. Bordé CJ. Quantum theory of atom-wave beam splitters and application to multidimensional atomic gravito-inertial sensors. *Gen Relativ Gravit*. 2004;36(3):475–502.
40. Barrett B, Cheiney P, Battelier B, Napolitano F, Bouyer P. Multidimensional atom optics and interferometry. *Phys Rev Lett*. 2019;122:043604.
41. Herrmann S, Göklü E, Müntinga H, Resch A, Van Zoest T, Dittus H et al. Testing fundamental physics with degenerate quantum gases in microgravity. *Microgravity Sci Technol*. 2010;22(4):529–38.
42. Bongs K, Holynski M, Vovrosh J, Bouyer P, Condon G, Rasel E et al. Taking atom interferometric quantum sensors from the laboratory to real-world applications. *Nat Rev Phys*. 2019;1:731.
43. Amelino-Camelia G, Lämmerzahl C, Mercati F, Tino GM. Constraining the energy-momentum dispersion relation with Planck-scale sensitivity using cold atoms. *Phys Rev Lett*. 2009;103:171302.
44. Arvanitaki A, Graham PW, Hogan JM, Rajendran S, Van Tilburg K. Search for light scalar dark matter with atomic gravitational wave detectors. *Phys Rev D*. 2018;117:075020.
45. Geraci AA, Derevianko A. Sensitivity of atom interferometry to ultralight scalar field dark matter. *Phys Rev Lett*. 2016;117:261301.
46. Rosi G, D'Amico G, Cacciapuoti L, Sorrentino F, Prevedelli M, Zych M et al. Quantum test of the equivalence principle for atoms in coherent superposition of internal energy states. *Nat Commun*. 2017;8:15529.
47. Duan XC, Deng XB, Zhou MK, Zhang K, Xu WJ, Xiong F et al. Test of the universality of free fall with atoms in different spin orientations. *Phys Rev Lett*. 2016;117:023001.
48. Zhou L, Long S, Tang B, Chen X, Gao F, Peng W et al. Test of equivalence principle at 10<sup>-8</sup> level by a dual-species double-diffraction Raman atom interferometer. *Phys Rev Lett*. 2015;115(1):1.
49. Bonnin A, Zahzam N, Bidel Y, Bresson A. Simultaneous dual-species matter-wave accelerometer. *Phys Rev Lett A*. 2013;88(4):043615.
50. Tarallo MG, Mazzoni T, Poli N, Sutyryn DV, Zhang X, Tino GM. Test of Einstein equivalence principle for 0-spin and half-integer-spin atoms: search for spin-gravity coupling effects. *Phys Rev Lett*. 2014;113(2):023005.
51. Xu V, Jaffe M, Panda CD, Kristensen SL, Clark LW, Müller H. Probing gravity by holding atoms for 20 seconds. *Science*. 2019;336:745.
52. Savoie D, Altorio M, Fang B, Sidorenkov LA, Geiger R, Landragin A. Interleaved atom interferometry for high-sensitivity inertial measurements. *Sci Adv*. 2018;4:eaau7948.
53. Dutta I, Savoie D, Fang B, Venon B, Garrido Alzar CL, Geiger R et al. Continuous cold-atom inertial sensor with 1 nrad/sec rotation stability. *Phys Rev Lett*. 2016;116:183003.
54. Berg P, Abend S, Tackmann G, Schubert C, Giese E, Schleich WP et al. Composite-light-pulse technique for high-precision atom interferometry. *Phys Rev Lett*. 2015;114:063002.
55. Stockton JK, Takase K, Kasevich MA. Absolute geodetic rotation measurement using atom interferometry. *Phys Rev Lett*. 2011;107:133001.
56. Bidel Y, Zahzam N, Bresson A, Blanchard C, Cadoret M, Olesen AV et al. Absolute airborne gravimetry with a cold atom sensor. *J Geod*. 2020;94(2):20.
57. Wu W, Pagel W, Malek BS, Nguyen TH, Zi F, Scheirer DS et al. Gravity surveys using a mobile atom interferometer. *Sci Adv*. 2019;5:eaau0800.
58. Ménoret V, Vermeulen P, Le Moigne N, Bonvalot S, Bouyer P, Landragin A et al. Gravity measurements below 10<sup>-9</sup> g with a transportable absolute quantum gravimeter. *Sci Rep*. 2018;8(1):12300.
59. Freier C, Hauth M, Schkolnik V, Leykauf B, Schilling M, Wziontek H et al. Mobile quantum gravity sensor with unprecedented stability. *J Phys Conf Ser*. 2016;723:012050. 8th Symposium on Frequency Standards and Metrology 2015 12–16 October 2015, Potsdam, Germany.
60. Hu ZK, Sun BL, Duan XC, Zhou MK, Chen LL, Zhan S et al. Demonstration of an ultrahigh-sensitivity atom-interferometry absolute gravimeter. *Phys Rev Lett*. 2013;88:043610.
61. Louchet-Chauvet A, Farah T, Bodart Q, Clairon A, Landragin A, Merlet S et al. The influence of transverse motion within an atomic gravimeter. *New J Phys*. 2011;13(6):065025.
62. Peters A, Chung KY, Chu S. Measurement of gravitational acceleration by dropping atoms. *Nature*. 1999;400:849–52.
63. Cheiney P, Fouché L, Templier S, Napolitano F, Battelier B, Bouyer P et al. Navigation-compatible hybrid quantum accelerometer using a Kalman filter. *Phys Rev Appl*. 2018;10:034030.
64. Jekeli C. Navigation error analysis of atom interferometer inertial sensor. *Navigation*. 2005;52:1.
65. Pandey S, Mas H, Drougakis G, Thekkeppatt P, Bolpasi V, Vasilakis G et al. Hypersonic Bose–Einstein condensates in accelerator rings. *Nature*. 2019;570:205–9.
66. Zhai Y, Carson CHH, Henderson VAA, Griffin PFF, Riis E, Arnold ASS. Talbot-enhanced, maximum-visibility imaging of condensate interference. *Optica*. 2018;5(1):80.
67. McDonald GD, Keal H, Altin PA, Debs JE, Bennetts S, Kuhn CCN et al. Optically guided linear Mach-Zehnder atom interferometer. *Phys Rev A*. 2013;87:013632.
68. Andia M, Jannin R, Nez F, Biraben F, Guellati-Khélifa S, Cladé P. Compact atomic gravimeter based on a pulsed and accelerated optical lattice. *Phys Rev A*. 2013;88:031605.
69. Charriere R, Cadoret M, Zahzam N, Bidel Y, Bresson A. Local gravity measurement with the combination of atom interferometry and Bloch oscillations. *Phys Rev A*. 2012;85(1):013639.

70. Su EJ, Wu S, Prentiss MG. Atom interferometry using wave packets with constant spatial displacements. *Phys Rev A*. 2010;81:043631.
71. Rosi G, Sorrentino F, Cacciapiuoti L, Prevedelli M, Tino G. Precision measurement of the Newtonian gravitational constant using cold atoms. *Nature*. 2014;510(7506):518–21.
72. Hartwig J, Abend S, Schubert C, Schlippert D, Ahlers H, Posso-Trujillo K et al. Testing the universality of free fall with rubidium and ytterbium in a very large baseline atom interferometer. *New J Phys*. 2015;17(3):1.
73. Kasevich M, Chu S. Atomic interferometry using stimulated Raman transitions. *Phys Rev Lett*. 1991;67:181–4.
74. Lepoutre S, Lonij VPA, Jelassi H, Tréneç G, Büchner M, Cronin AD et al. Atom interferometry measurement of the atom-surface van der Waals interaction. *Eur Phys J D*. 2011;62(3):309–25.
75. Alauze X, Bonnin A, Solaro C, Santos FPD. A trapped ultracold atom force sensor with a  $\mu\text{m}$ -scale spatial resolution. *New J Phys*. 2018;20(8):083014.
76. Trimeche A, Battelier B, Becker D, Bertoldi A, Bouyer P, Braxmaier C et al. Concept study and preliminary design of a cold atom interferometer for space gravity gradiometry. *Class Quantum Gravity*. 2019;36:215004.
77. Douch K, Wu H, Schubert C, Müller J, dos Santos FP. Simulation-based evaluation of a cold atom interferometry gradiometer concept for gravity field recovery. *Adv Space Res*. 2018;61:1307.
78. Carraz O, Siemes C, Massotti L, Haagmans R, Silvestrin P. A spaceborne gravity gradiometer concept based on cold atom interferometers for measuring Earth's gravity field. *Microgravity Sci Technol*. 2014;26:139.
79. Tino GM et al. Precision gravity tests with atom interferometry in space. *Nucl Phys B, Proc Suppl*. 2013;243(244):203–17.
80. Aguilera D et al. STE-QUEST - test of the universality of free fall using cold atom interferometry. *Class Quantum Gravity*. 2014;31:115010.
81. Williams J et al. Quantum test of the equivalence principle and space-time aboard the International Space Station. *New J Phys*. 2016;18:025018.
82. Fixler JB, Foster GT, McGuirk JM, Kasevich MA. Atom interferometer measurement of the Newtonian constant of gravity. *Science*. 2007;315:74.
83. Hohensee MA, Estey B, Hamilton P, Zeilinger A, Müller H. Force-free gravitational redshift: proposed gravitational Aharonov-Bohm experiment. *Phys Rev Lett*. 2012;108:230404.
84. Hogan JM, Kasevich MA. Atom-interferometric gravitational-wave detection using heterodyne laser links. *Phys Rev A*. 2016;94:033632.
85. Hogan JM et al. An atomic gravitational wave interferometric sensor in low Earth orbit (AGIS-LEO). *Gen Relativ Gravit*. 2011;43:1953.
86. Dimopoulos S, Graham PW, Hogan JM, Kasevich MA, Rajendran S. Atomic gravitational wave interferometric sensor. *Phys Rev D*. 2008;78:122002.
87. Rudolph J. Matter-Wave optics with Bose-Einstein condensates in microgravity [Dissertation]. Leibniz Universität Hannover; 2016.
88. Kovachy T, Hogan JM, Sugarbaker A, Dickerson SM, Donnelly CA, Overstreet C et al. Matter wave lensing to picokelvin temperatures. *Phys Rev Lett*. 2015;114:143004.
89. Inouye S, Andrews MR, Stenger J, Miesner HJ, Stamper-Kurn DM, Ketterle W. Observation of Feshbach resonances in a Bose-Einstein condensate. *Nature*. 1998;392(6672):151–4.
90. Chin C, Grimm R, Julienne P, Tiesinga E. Feshbach resonances in ultracold gases. *Rev Mod Phys*. 2010;82:1225–86.
91. Qin J. Non-spread matter-wave packets in a ring. *Phys Scr*. 2019;94(11):115402.
92. McDonald GD, Kuhn CCN, Hardman KS, Bennetts S, Everitt PJ, Altin PA et al. Bright solitonic matter-wave interferometer. *Phys Rev Lett*. 2014;113:013002.
93. Pasquini TA, Saba M, Jo GB, Shin Y, Ketterle W, Pritchard DE et al. Low velocity quantum reflection of Bose-Einstein condensates. *Phys Rev Lett*. 2006;97(9):093201.
94. Olf R, Fang F, Marti GE, MacRae A, Stamper-Kurn DM. Thermometry and cooling of a Bose gas to 0.02 times the condensation temperature. *Nat Phys*. 2015;11(9):720–3.
95. Chu S, Bjorkholm J, Ashkin A, Cable A. Experimental observation of optically trapped atoms. *Phys Rev Lett*. 1986;57(3):314.
96. Stamper-Kurn DM, Andrews MR, Chikkatur AP, Inouye S, Miesner HJ, Stenger J et al. Optical confinement of a Bose-Einstein condensate. *Phys Rev Lett*. 1998;80(10):2027–30.
97. Baranov MA. Theoretical progress in many-body physics with ultracold dipolar gases. *Phys Rep*. 2008;464(3):71–111.
98. Stamper-Kurn DM, Ueda M. Spinor Bose gases: symmetries, magnetism, and quantum dynamics. *Rev Mod Phys*. 2013;85(3):1191–244.
99. Roberts JL, Claussen NR, Cornish SL, Wieman CE. Magnetic field dependence of ultracold inelastic collisions near a Feshbach resonance. *Phys Rev Lett*. 2000;85(4):728–31.
100. Petrov DS. Quantum mechanical stabilization of a collapsing Bose-Bose mixture. *Phys Rev Lett*. 2015;115(15):155302.
101. Cabrera CR, Tanzi L, Sanz J, Naylor B, Thomas P, Cheiney P et al. Quantum liquid droplets in a mixture of Bose-Einstein condensates. *Science*. 2018;359(6373):301–4.
102. Semeghini G, Ferioli G, Masi L, Mazzinghi C, Wolswijk L, Minardi F et al. Self-bound quantum droplets of atomic mixtures in free space. *Phys Rev Lett*. 2018;120(23):235301.
103. D'Incao JP, Krutzik M, Elliott E, Williams JR. Enhanced association and dissociation of heteronuclear Feshbach molecules in a microgravity environment. *Phys Rev A*. 2017;95(1):012701.
104. Braaten E, Hammer HW. Universality in few-body systems with large scattering length. *Phys Rep*. 2006;428(5):259–390.
105. Naidon P, Endo S. Efimov physics: a review. *Rep Prog Phys*. 2017;80(5):056001.
106. Northup TE, Blatt R. Quantum information transfer using photons. *Nat Photonics*. 2014;8(5):356–63.
107. Lvovsky AI, Sanders BC, Tittel W. Optical quantum memory. *Nat Photonics*. 2009;3(12):706–14.
108. Bedington R, Arrazola JM, Ling A. Progress in satellite quantum key distribution. *npj Quantum Information*. 2017;3(1):30.
109. Liao SK, Cai WQ, Handsteiner J, Liu B, Yin J, Zhang L et al. Satellite-relayed intercontinental quantum network. *Phys Rev Lett*. 2018;120:030501.

110. Ma L, Slattery O, Tang X. Optical quantum memory based on electromagnetically induced transparency. *J Opt.* 2017;19(4):043001.
111. NASA. SSP57000 pressurized payloads interface requirements document. International Space Station Program; 2018.
112. NASA. SSP51700 payload safety policy and requirements for the ISS. International Space Station Program; 2010.
113. Kubelka-Lange A, Herrmann S, Grosse J, Lämmerzahl C, Rasel EM, Braxmaier C. A three-layer magnetic shielding for the MAIUS-1 mission on a sounding rocket. *Rev Sci Instrum.* 2016;87(6):063101.
114. Haslinger P, Jaffe M, Xu V, Schwartz O, Sonnleitner M, Ritsch-Marte M et al. Attractive force on atoms due to blackbody radiation. *Nat Phys.* 2018;14(3):257–60.
115. Piest B, Bartosch W, Becker D, Böhm J, Döringshof K, Elsen M et al. MAIUS-2/-3: a system for two-species atom interferometry in space. In: Proceedings of the 24th ESA symposium on European ROCKET & BALLOON programmes and related research (2019); 2020.
116. Chaudhuri S, Roy S, Unnikrishnan CS. Realization of an intense cold Rb atomic beam based on a two-dimensional magneto-optical trap: experiments and comparison with simulations. *Phys Rev A.* 2006;74(2):1.
117. Zobay O, Garraway BM. Two-dimensional atom trapping in field-induced adiabatic potentials. *Phys Rev Lett.* 2001;86:1195–8.
118. Heathcote WH, Nugent E, Sheard BT, Foot CJ. A ring trap for ultracold atoms in an RF-dressed state. *New J Phys.* 2008;10:043012.
119. Morizot O, Colombe Y, Lorent V, Perrin H, Garraway BM. Ring trap for ultracold atoms. *Phys Rev A.* 2006;74:023617.
120. Lévêque T, Gauguier A, Michaud F, Pereira Dos Santos F, Landragin A. Enhancing the area of a Raman atom interferometer using a versatile double-diffraction technique. *Phys Rev Lett.* 2009;103(8):080405.
121. Roura A, Zeller W, Schleich WP. Overcoming loss of contrast in atom interferometry due to gravity gradients. *New J Phys.* 2014;16(12):123012.
122. Lan SY, Kuan PC, Estey B, Haslinger P, Müller H. Influence of the Coriolis force in atom interferometry. *Phys Rev Lett.* 2012;108(9):090402.
123. Roura A. Circumventing Heisenberg's uncertainty principle in atom interferometry tests of the equivalence principle. *Phys Rev Lett.* 2017;118:160401.
124. Overstreet C, Asenbaum P, Kovachy T, Notermans R, Hogan JM, Kasevich MA. Effective inertial frame in an atom interferometric test of the equivalence principle. *Phys Rev Lett.* 2018;120:183604.
125. Roura A. Compensation of gravity gradients and rotations in precision atom interferometry. In: 656th WE-Heraeus-seminar: fundamental physics in space. Bremen; 2017. p. 29–35. <https://www.zarm.uni-bremen.de/fps2017/download.html>.
126. Franke-Arnold S, Leach J, Padgett MJ, Lembessis VE, Ellinas D, Wright AJ et al. Optical ferris wheel for ultracold atoms. *Opt Express.* 2007;15(14):8619.
127. Henderson K, Ryu C, MacCormick C, Boshier MG. Experimental demonstration of painting arbitrary and dynamic potentials for Bose-Einstein condensates. *New J Phys.* 2009;11(4):1.
128. Trypogeorgos D, Harte T, Bonnin A, Foot C. Precise shaping of laser light by an acousto-optic deflector. *Opt Express.* 2013;21(21):24837.
129. Bell TA, Glidden JAP, Humbert L, Bromley MWJ, Haine SA, Davis MJ et al. Bose-Einstein condensation in large time-averaged optical ring potentials. *New J Phys.* 2016;18(3):035003.
130. Bruce GD, Mayoh J, Smirne G, Torralbo-Campo L, Cassetari D. A smooth, holographically generated ring trap for the investigation of superfluidity in ultracold atoms. *Phys Scr.* 2011;T143(T143):014008.
131. Lee JG, Hill WT. Spatial shaping for generating arbitrary optical dipole traps for ultracold degenerate gases. *Rev Sci Instrum.* 2014;85(10):103106.
132. Wieman CE, Hollberg L. Using diode lasers for atomic physics. *Rev Sci Instrum.* 1991;62(1):1–20.
133. Schkolnik V, Hellmig O, Wenzlawski A, Grosse J, Kohfeldt A, Döringshoff K et al. A compact and robust diode laser system for atom interferometry on a sounding rocket. *Appl Phys B.* 2016;122(8):7.
134. Pahl J, Dinkelaker AN, Grzeschik C, Kluge J, Schiemangk M, Wicht A et al. Compact and robust diode laser system technology for dual-species ultracold atom experiments with rubidium and potassium in microgravity. *Appl Opt.* 2019;58(20):5456.
135. Lezius M, Wilken T, Deutsch C, Giunta M, Mandel O, Thaller A et al. Space-borne frequency comb metrology. *Optica.* 2016;3(12):1381.
136. Wicht A, Bawamia A, Krüger M, Kürbis C, Schiemangk M, Smol R et al. Narrow linewidth diode laser modules for quantum optical sensor applications in the field and in space. In: Glebov AL, Leisher PO, editors. Components and packaging for laser systems III. vol. 10085; 2017. 100850F.
137. Schiemangk M, Lampmann K, Dinkelaker A, Kohfeldt A, Krutzik M, Kürbis C et al. High-power, micro-integrated diode laser modules at 767 and 780 nm for portable quantum gas experiments. *Appl Opt.* 2015;54(17):5332.
138. Mihm M, Marburger JP, Wenzlawski A, Hellmig O, Anton O, Döringshoff K et al. ZERODUR® based optical systems for quantum gas experiments in space. *Acta Astronaut.* 2019;159:166–9.
139. Luvsandamdin E, Spießberger S, Schiemangk M, Sahm A, Mura G, Wicht A et al. Development of narrow linewidth, micro-integrated extended cavity diode lasers for quantum optics experiments in space. *Appl Phys B.* 2013;111(2):255–60.
140. Luvsandamdin E, Kürbis C, Schiemangk M, Sahm A, Wicht A, Peters A et al. Micro-integrated extended cavity diode lasers for precision potassium spectroscopy in space. *Opt Express.* 2014;22(7):7790.
141. Kürbis C, Bawamia A, Krüger M, Smol R, Peters A, Wicht A et al. Extended cavity diode laser master-oscillator-power-amplifier for operation of an iodine frequency reference on a sounding rocket. *Appl Opt.* 2020;59(2):253.
142. Di Domenico G, Schilt S, Thomann P. Simple approach to the relation between laser frequency noise and laser line shape. *Appl Opt.* 2010;49(25):4801.
143. Duncker H, Hellmig O, Wenzlawski A, Grote A, Rafipoor AJ, Rafipoor M et al. Ultrastable, Zerodur-based optical benches for quantum gas experiments. *Appl Opt.* 2014;53(20):4468.

144. Marburger JP, Mihm M, Hellmig O, Wenzlawski A, Windpassinger P. Highly stable Zerodur based optical benches for microgravity applications and other adverse environments. In: International conference on space optics — ICSSO 2018. Proceedings SPIE. vol. 11180; 2019:181.
145. Weps B, Lüdtko D, Franz T, Maibaum O, Wendrich T, Müntinga H et al. A model-driven software architecture for ultra-cold gas experiments in space. In: 69th international astronomical congress (IAC); 2018.

**Submit your manuscript to a SpringerOpen<sup>®</sup> journal and benefit from:**

- ▶ Convenient online submission
- ▶ Rigorous peer review
- ▶ Open access: articles freely available online
- ▶ High visibility within the field
- ▶ Retaining the copyright to your article

---

Submit your next manuscript at ▶ [springeropen.com](https://www.springeropen.com)

---